ORNL
MASTER COPY
EXTERNAL TRANSMITTAL AUTHORIZED
69

ORNL
Central Files Number
60-4-12

161

CRITICAL EXPERIMENTS FOR REACTOR PHYSICS STUDIES

R. Gwin
D. W. Magnuson

[redacted]

[redacted]

OAK RIDGE NATIONAL LABORATORY
operated by
UNION CARBIDE CORPORATION
for the
U.S. ATOMIC ENERGY COMMISSION

LEGAL NOTICE

This report was prepared as an account of Government sponsored work. Neither the United States, nor the Commission, nor any person acting on behalf of the Commission:

A. Makes any warranty or representation, expressed or implied, with respect to the accuracy, completeness, or usefulness of the information contained in this report, or that the use of any information, apparatus, method, or process disclosed in this report may not infringe privately owned rights; or

B. Assumes any liabilities with respect to the use of, or for damages resulting from the use of any information, apparatus, method, or process disclosed in this report.

As used in the above, "person acting on behalf of the Commission" includes any employee or contractor of the Commission, or employee of such contractor, to the extent that such employee or contractor of the Commission, or employee of such contractor prepares, disseminates, or provides access to, any information pursuant to his employment or contract with the Commission, or his employment with such contractor.

External Transmittal
Authorized
ORNL
Central Files Number

60-4-12

Critical Experiments for Reactor Physics Studies

R. Gwin and D. W. Magnuson

Date Issued

SEP 1 6 1960

OAK RIDGE NATIONAL LABORATORY
Operated by
UNION CARBIDE NUCLEAR COMPANY
Post Office Box X
Oak Ridge, Tennessee

TABLE OF CONTENTS

	Page No.
Abstract	iii
Introduction	1
Theoretical Considerations	2
Critical Equation	2
Epithermal Flux Parameter	4
Nonleakage Probability	5
Calculations of Steady State Flux Distribution	9
Experimental Results	12
Critical Experiments	12
Buckling Measurements and Extrapolation Distances	12
Cross Sections Needed for Calculations	13
Foil Measurements of the Epithermal Flux	17
Experimental Determination of Nonleakage Probabilities	18
Calculation of Eta from Critical Experiments	28
Supplementary Data	33
Error Analysis	33
Summary	36
Acknowledgements	37
Appendix A: Experimental Details	38
Appendix B: Foil Measurements	46
Appendix C: Period Observations	47
References	60

ABSTRACT

The thermal value of $\bar{\eta}$ for U^{233} and for U^{235} has been determined in a series of experiments involving direct comparison of the critical parameters of unreflected homogeneous aqueous solutions of the two isotopes. Auxiliary experiments establishing limits of error, testing certain aspects of the theoretical model employed, and experimentally determining the parameters in the critical equation, have been performed. Experiments performed with 27-in.-dia and 48-in.-dia spheres, and 5-ft-dia and 9-ft-dia cylinders have yielded consistent values of η. Measurements of the nonleakage probability in cylindrical geometry have given values consistent with those predicted by a two-group model in which the theoretical value of the age was used. Within the experimental error no differences were found in the ages of fission neutrons for U^{233} and U^{235}.

The average thermal values of eta determined are: $\bar{\eta}$ for U^{233}, 2.284 ± 0.015 and $\bar{\eta}$ for U^{235}, 2.074 ± 0.015. The 2200 m/sec values are the same since the g-factors for eta are unity.

INTRODUCTION

The importance of and necessity for a precise determination of the thermal value of η for U^{233}, the number of fission neutrons produced per thermal neutron absorbed in the fissile isotope, has been so sufficiently and widely emphasized in recent months that further discussion is redundant. An experimental determination of this value, based on the direct comparison of the critical parameters of unreflected homogeneous aqueous solutions of the uranyl nitrates of U^{233} and U^{235}, has been made. The precision achieved by this method, earlier employed by Thomas, Fox and Callihan,[1] is enhanced by the use of dilute solutions in large systems. In such systems the number of epithermal fissions and absorptions is reduced and the uncertainties in the evaluation of the neutron leakage are minimized. In the present investigation, therefore, the largest volumes consistent with the amount of U^{233} available have been used.

Supplementary experiments, primarily required to establish limits of error on the measured value of $\bar{\eta}$, have verified several aspects of the theoretical model for the bare homogeneous reactor. The experimental program consisted of the following:

1. Experiments in which the critical dimensions of both spherical and cylindrical volumes of aqueous solutions of U^{233} and U^{235} were measured as functions of the chemical concentration and directly compared. In one of these comparisons boron was added to the U^{233} solution to equate the total macroscopic absorption cross section to that of the U^{235} solution, in an attempt to more closely match the spectra. Boron was also added to some of the U^{235} solutions with the intention of examining the internal consistency of the various cross sections. However, the neutron spectrum changed rapidly as the boron and U^{235} concentrations were increased, and it soon became apparent that any evaluation of the relative cross sections would be obscured by spectral uncertainties. The data were valuable, nevertheless, in studying the theoretical model.

2. Flux traverses, using U^{235}, U^{238}, and cadmium-covered U^{235} miniature fission counters, and in one case a gold wire, were made to define the buckling, B^2, or the shape of the neutron flux, so that an extrapolation distance could be obtained.

3. The effects of the epithermal neutron flux, the measurement of which is an important and difficult field of reactor physics, were expressed in this work in integral form. The experimental determinations were made from fission foil activations, using both bare and cadmium-covered foils of both U^{233} and U^{235}.

4. Kinetic experiments, in which the stable period resulting from an incremental addition of solution to a critical cylinder was measured,

were performed to experimentally determine nonleakage probabilities and furnish information regarding the age of fission neutrons in the solutions.

The experimental investigations have been supported by theoretical calculations using the Corn Pone Code,[2] and detailed calculations were made of the flux and boundary conditions in a 69.2-cm-dia sphere, where the neutron leakage was great enough to be significant.

THEORETICAL CONSIDERATIONS

Critical Equation

The theoretical analysis of chain reacting homogeneous water-moderated assemblies is based upon the theory presented by Weinberg and Wigner.[3] Since an extension of this theory using a measured slowing-down kernel with consideration of epithermal absorption has been presented previously[4] only a brief outline of the theory is presented here, beginning with two basic theorems.

The First Fundamental Theorem of Reactor Theory states that the stationary neutron distribution $\Phi(\vec{x},E)$ in a critical bare reactor is separable in space and energy, i.e.,

$$\Phi(\vec{x},E) = \phi(E)\psi(\vec{x})$$

where the spatial distribution, $\psi(\vec{x})$, is the fundamental solution of the wave equation,

$$\nabla^2\psi(\vec{x}) + B^2\psi(\vec{x}) = 0$$

that is, that solution which is positive throughout the reactor and vanishes on the extrapolated boundary.

If the neutron flux satisfies the wave equation and if the point slowing-down kernel is an isotropic displacement kernel, then the second fundamental theorem of reactor theory states that the nonescape probability of neutrons during moderation in a uniform bare reactor is the Fourier transform of the slowing down kernel. Since the slowing down kernel in a bare reactor will change in form near the boundary, the theory cannot be expected to give a detailed description of the neutron flux as a function of position and energy near the boundary. If there exists a region about the center of systems having sufficiently small values of B^2 in which the fluxes at all energies do have the same shape, then it is possible to formulate the critical conditions for that reactor using these fundamental theorems.

The above concepts lead to the following equation for the balance of neutrons in the thermal energy group, assuming no absorption over the fission spectrum:

$$-\bar{D}\, B^2 \psi(\vec{x}) - \bar{\Sigma}_{at}\, \psi(\vec{x}) + K(B,E_{th})\, p(E_{th})\, \psi(\vec{x}) \int_0^\infty \phi(E')\Sigma_f(E')\,\nu(E')dE' = 0 \qquad (1)$$

in which

Overscore = Maxwellian-flux-average values,
$\bar{D}$ = thermal diffusion coefficient,
B^2 = buckling,
$\bar{\Sigma}_{at}$ = total thermal neutron macroscopic absorption cross section,
$K(B,E)$ = nonleakage probability during slowing down to energy E,
$p(E)$ = probability that a neutron will not be absorbed during slowing down to energy E,
$\Sigma_f(E)$ = macroscopic fission cross section,
$\nu(E)$ = average number of neutrons produced per fission.

The spectral distribution of the neutron flux was assumed to be Maxwellian at the system temperature of 24° - 25°C, in the region of thermal energies, supplemented above 0.2 ev by a component nearly inversely proportional to the energy. The following relations were used to describe this distribution:

$\phi(E) = \phi_M$ = Maxwellian flux for $0 \leq E \leq 0.2$ ev,

$\phi(E) = \dfrac{\lambda(E)}{E} + \phi_M$ for $0.2 \leq E \leq 10^6$ ev,

$\lambda(E)$ = proportionality constant relating the Maxwellian spectrum to the epithermal 1/E spectrum,

ϕ_M is normalized so that $\int_0^\infty \phi(M)dE = 1$

The term $\lambda(E)$ is defined by

$$\lambda(E) = \frac{K(B,E)}{\xi\,\Sigma_t(E)}\, p(E) \int_0^\infty \phi(E')\, \Sigma_f(E')\, \nu(E')dE' \qquad (2)$$

in which ξ is the logarithmic energy decrement and $\Sigma_t(E)$ is the total macroscopic cross section.

The absorption escape probability to thermal energy is:

$$p(E_{th}) = \frac{\int_0^\infty \phi_M(E)\, \Sigma_{at}(E)dE}{\int_0^\infty \phi_M(E)\, \Sigma_{at}(E)dE + \int_{0.2}^\infty \frac{\lambda(E)}{E}\, \Sigma_{at}(E)dE} \qquad (3)$$

From these relations the critical equation becomes

$$k_{eff} = \frac{K(B,E_{th})}{1 + L^2B^2} \quad p(E_{th})\ \bar{\eta}\ \frac{\Sigma_{ax}}{\Sigma_{at}}\ \epsilon = 1 \tag{4}$$

in which $\bar{\Sigma}_{ax}$ = Maxwellian-flux-averaged macroscopic absorption cross section of the fissile isotope and

$$\epsilon = \text{fast fission factor} = 1 + \frac{\int_{0.2\ ev}^{\infty} \frac{\lambda(E)}{E}\ \nu(E)\ \Sigma_f(E)dE}{\bar{\eta}\ \bar{\Sigma}_{ax}}$$

By defining:

$$P(B) = \frac{K(B,E_{th})}{1 + L^2B^2},$$

f = thermal utilization, and

$F = \epsilon\ p(E_{th})$,

the critical equation becomes:

$$k_{eff} = P(B)\ f\ \bar{\eta}\ F = 1 \tag{5}$$

In the above development it is seen that P(B) is the fraction of the source neutrons which do not escape the system. The detailed effect of the absorptions and leakage of epithermal neutrons as a function of energy then appears in the neutron flux, $\frac{\lambda(E)}{E}$, and the quantity, $K(B,E_{th})$, in the critical equation is the Fourier transform of the point slowing-down kernel to thermal energy.

Epithermal Flux Parameter

The activations of bare and cadmium-covered fission foils in the critical system, A_{bare} and A_{cd} respectively, are used to evaluate the epithermal (> 0.4 ev) source of fission neutrons in terms of the total source. The equation used is:

$$\frac{A_{bare}}{A_{cd}} = \frac{\int_0^{\infty} \phi_M\ \Sigma_{act}dE + \int_{0.2}^{\infty} \lambda(E)\ \frac{\Sigma_{act}}{E}\ dE}{\int_{0.4}^{\infty} \lambda(E)\ \frac{\Sigma_{act}}{E}\ dE} \tag{6}$$

In the energy region between 0.2 and 0.4 ev the source of fission neutrons must be theoretically estimated. The epithermal source permits an average value of λ to be obtained from the expression

$$\lambda \int_{0.4\ ev}^{\infty} \frac{\Sigma_f(E)}{E} \nu(E)dE = \int_{0.4\ ev}^{\infty} \frac{\lambda(E)}{E} \Sigma_f(E) \nu(E)dE \qquad (7)$$

This value of λ can be applied also to the absorption integral within the limits imposed by the assumption that the ratio of the absorption and fission cross sections is constant with energy, thereby yielding an approximation of the epithermal parasitic neutron capture. The error limits were estimated theoretically to be ± 2%.

The assumed form of the flux has been compared with that measured by Poole[5] and by Stone and Slovacek[6] in the region where the transition from Maxwellian to the 1/E distribution occurs. It has been found that the assumed form yields total U^{235} activation integrals which differ by about 2% from those based on above measured distributions.

Nonleakage Probability

The nonleakage probability during slowing down is given by the Fourier transform of the point slowing down kernel in an infinite medium. This probability can be written in moments of $\overline{r^n}$ which are defined by the relation

$$\overline{r^n} = \frac{\int_0^{\infty} G(r)\ r^n\ 4\pi r^2 dr}{\int_0^{\infty} G(r)\ 4\pi r^2 dr} \qquad (8)$$

in which G(r) is the slowing-down kernel. The nonleakage probability becomes

$$K(B) = \sum_{i=0}^{\infty} \frac{(-1)^i\ B^{2i}\ \overline{r^{2i}}}{(2i+1)!} \qquad (9)$$

By using the values of $\overline{r^{2i}}$ calculated by Certaine and Aronson[7] for a distribution of fission neutrons to indium resonance energy, the nonleakage probability is

$$K(B) = 1 - 25.67\ B^2 + 815.8\ B^4 - 3.837 \times 10^4\ B^6 + 2.412 \times 10^6\ B^8 \qquad (10)$$

A representation of K(B) satisfactory to within 0.2% for $B^2 \leqslant 0.004\ cm^{-2}$ and satisfactory to within 0.5% for $B^2 \leq 0.007\ cm^{-2}$ can be written as

$$K(B) = \frac{1}{1 + \tau B^2} \quad \text{where} \quad \tau = 25.67\ cm^2 \qquad (11)$$

This equivalence was used for simplicity in the experimental evaluation of the nonleakage probability described below.

The critical equation is of the form

$$k_{eff} = \bar{\eta}\ f\ F\ P(B) = k_\infty\ P(B) \qquad (12)$$

and its differential for buckling perturbations is:

$$\Delta k_{eff} = k_\infty \frac{\partial P(B)}{\partial B^2} \Delta B^2. \qquad (13)$$

Further, the kinetic relation connecting the stable reactor period to the change in k_{eff} from unity yields, neglecting the term $\frac{\ell}{T}$,

$$\Delta k_{eff} = k_\infty\ P_d(B) \sum_i \frac{\beta_i}{1 + \lambda_i T} \qquad (14)$$

in which

β_i = fraction of fission neutrons in the delayed group i,
λ_i = decay constant of the precursors of the ith group of delayed neutrons,
ℓ = neutron lifetime,
T = stable reactor period,
$P_d(B)$ = average nonleakage probability of delayed neutrons.

From these equations

$$\frac{\partial P(B)}{\partial B^2} = P_d(B) \frac{\sum_i \frac{\beta_i}{1 + \lambda_i T}}{\Delta B^2} = -N. \qquad (15)$$

The nonleakage probability, $P(B_o)$, for a system having buckling, B_o^2, can be obtained by a Taylor's expansion about the nonleakage probability, $P(B)$, having buckling, B^2. In general,

$$P(B_o) = P(B) + \left.\frac{\partial P(B)}{\partial B^2}\right|_B \Delta B^2 + \left.\frac{\partial^2 P(B)}{\partial B^4}\right|_B \frac{(\Delta B^2)^2}{2!} + \ldots \tag{16}$$

and for the infinite system, $P(B_o) = 1$,

$$1 = P(B) + \left.\frac{\partial P(B)}{\partial B^2}\right|_B (-B^2) + \left.\frac{\partial^2 P(B)}{\partial B^4}\right|_B \frac{B^4}{2!} + \ldots \tag{17}$$

Using this expansion, the nonleakage probability can be evaluated in terms of its derivatives.

If $P(B)$ can be represented by a one group model of the form

$$P(B) = \frac{1}{1 + M^2B^2},$$

in which M^2 = migration area = $L^2 + \tau$, then

$$P(B) = \frac{1}{2}\left[1 + \left(1 - 4B^2 N\right)^{1/2}\right]. \tag{18}$$

For a two group model

$$P(B) = \frac{1}{(1 + \tau B^2)(1 + L^2B^2)}, \tag{19}$$

and, to terms in B^4,

$$P(B) = \frac{1}{2}\left[1 + B^2 \frac{\partial P(B)}{\partial B^2}\right] + \frac{1}{2}\left\{\left[1 + B^2 \frac{\partial P(B)}{\partial B^2}\right]^2 - 2\left[B^2 \frac{\partial P(B)}{\partial B^2}\right]^2 A,\right\}^{1/2}$$

$$\text{where } A = 1 + \frac{\dfrac{\tau^2}{(1+\tau B^2)^2} + \dfrac{L^4}{(1+L^2B^2)^2}}{\left[\dfrac{\tau}{1+\tau B^2} + \dfrac{L^2}{1+L^2B^2}\right]^2}$$

Neglecting terms of higher order than B^4, this expression can be written as

$$P(B) = 1 + B^2 \frac{\partial P(B)}{\partial B^2} - \frac{\left[B^2 \dfrac{\partial P(B)}{\partial B^2}\right]^2 A}{2\left[1 + B^2 \dfrac{\partial P(B)}{\partial B^2}\right]} \tag{20}$$

without introducing an error greater than 0.1% provided that B^2 is 0.004 cm^{-2} or less.

An interesting relation can be obtained by rewriting Eq. 15 in the form

$$S(B) = \frac{-\sum_i \dfrac{\beta_i}{1+\lambda_i T}}{\Delta B^2} = -\frac{1}{P_d(B)} \cdot \frac{\partial P(B)}{\partial B^2} \tag{21}$$

and expressing P(B) in the form

$$P(B) = \frac{1}{\prod_i (1 + L_i^2 B^2)} .$$

Then

$$\frac{\partial P(B)}{\partial B^2} = -P(B) \sum_i \frac{L_i^2}{1 + L_i^2 B^2}$$

and, in the limit of $B^2 = 0$

$$\frac{\partial P(B)}{\partial B^2} = -\sum_i L_i^2 = -M^2 \tag{22}$$

where M^2 is the migration area of the critical system having zero buckling. Thus S(B) plotted as a function of B^2 yields, as the intercept, the value of

M^2. The age of fission neutrons to thermal energy can, therefore, be obtained from experimental bucklings.

Calculations of Steady State Flux Distribution

One of the critical volumes studied experimentally, a sphere of aqueous solutions of U^{235}, was treated analytically using the Corn Pone code.[2,8,9] Since this volume had the greatest buckling of all those examined in this series of experiments, this particular analysis was a test of the experimental method. The calculation first yielded the steady state neutron source and flux as functions of position and energy for various energy groups, with the condition of zero net inwardly directed neutron current at the extrapolated boundary.

The fluxes and sources in the energy groups were then satisfactorily fitted to the equations

$$\phi(r) = A_\phi \frac{\sin B_\phi r}{B_\phi r}$$

$$S(r) = A_s \frac{\sin B_s r}{B_s r}$$

by a least-squares fit to obtain values of B, the square root of the buckling.

These calculations were performed in steps which successively included larger volumes of the sphere until the boundary was reached and show that, while the pure $\frac{\sin Br}{Br}$ mode does not exist even near the center, the departure from this mode is very small. It was observed that the bucklings for the various energy groups were within a range of less than 0.3% when points within 9 cm of the boundary were omitted; the corresponding value of the extrapolation length, d, is 2.3 cm. The fact that the spatial distribution of the neutrons about the center of the reactor is not strongly dependent on their energy is significant in that, for larger systems, there is no reason to expect the effect of the boundary to be projected any further inside the surface than in this case. The conclusion is then that bare systems of small B^2 can be very useful in testing certain aspects of reactor theory. The value of the effective extrapolation length for the source and the flux for each of various energy groups is shown in Fig. 1. Data from the entire sphere were included in these evaluations. Table 1 shows the energy corresponding to each of the various groups.

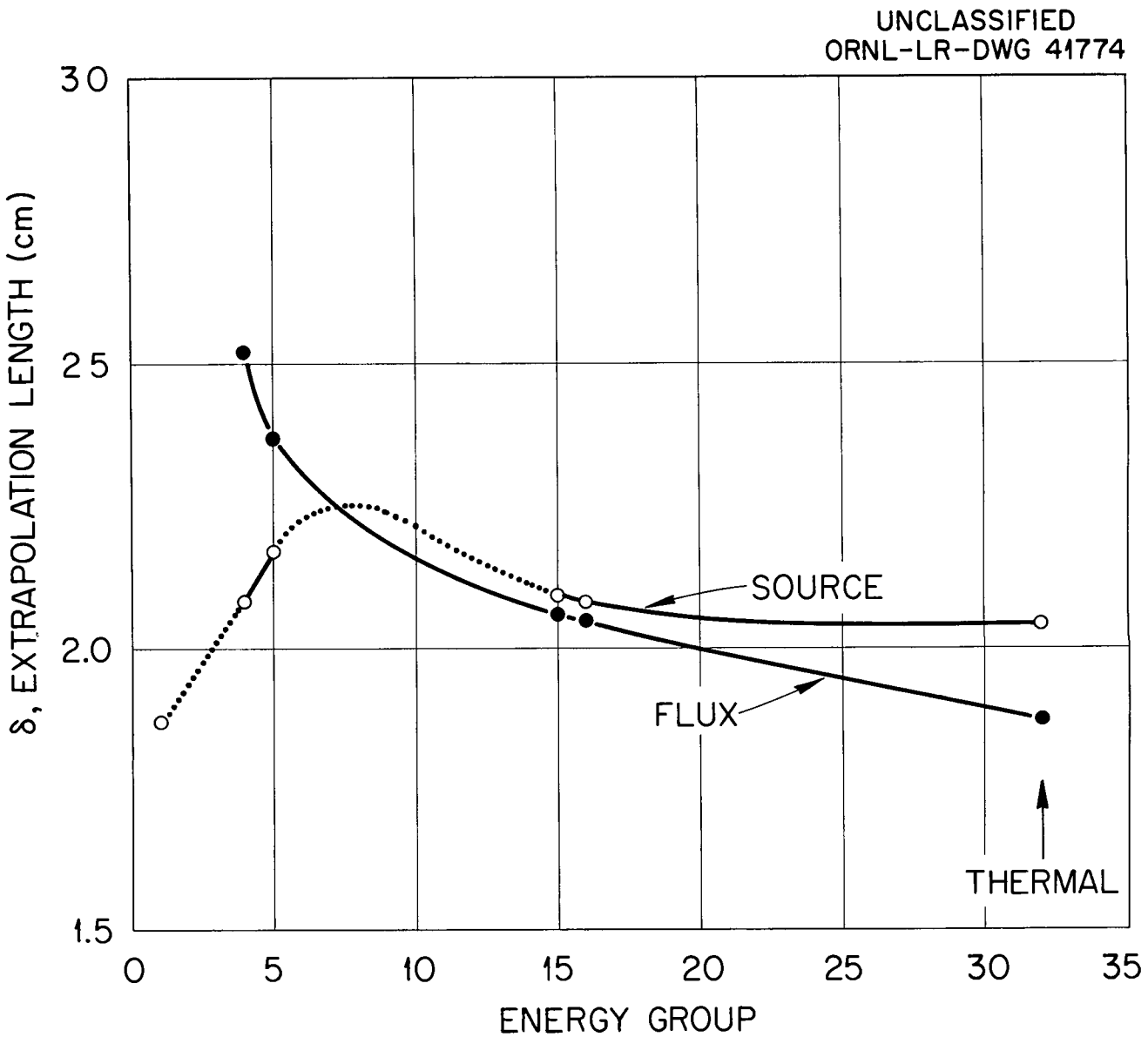

Fig. 1. Extrapolation Length as a Function of Energy Group

Table 1. Energy-Group Limits

Group	Lower Energy (ev)	Group	Lower Energy (ev)	Group	Lower Energy (ev)
	1×10^{8}	11	3.372×10^{1}	22	1.523×10^{-1}
1	1×10^{7}	12	1.515×10^{1}	23	1.247×10^{-1}
2	6.065×10^{6}	13	1.016×10^{1}	24	1.021×10^{-1}
3	3.679×10^{6}	14	4.564×10^{0}	25	8.358×10^{-2}
4	2.231×10^{6}	15	1.375×10^{0}	26	6.843×10^{-2}
5	1.353×10^{6}	16	9.214×10^{-1}	27	5.603×10^{-2}
6	8.208×10^{5}	17	6.176×10^{-1}	28	4.587×10^{-2}
7	1.832×10^{5}	18	4.140×10^{-1}	29	3.756×10^{-2}
8	9.118×10^{3}	19	2.775×10^{-1}	30	3.075×10^{-2}
9	4.54×10^{2}	20	2.272×10^{-1}	31	2.518×10^{-2}
10	1.12×10^{2}	21	1.860×10^{-1}	32	Thermal

A calculation was also performed to find the value of B which, when used for all energy groups, gave the same total nonleakage probability as in the previous case. The associated extrapolation distance is 2.4 cm, which compares favorably with the above value of 2.3 cm. However, the assumption of an energy-independent buckling can not describe the leakage in each energy group. In order to illustrate the effect of the boundary condition chosen and to compare the consistent P_1 solution with diffusion theory, a summary of the above calculations is shown in Table 2.

Table 2. Summary of Theoretical Calculations for a 34.6-cm-radius Sphere

Boundary Condition	Consistent P_1		Diffusion Theory	
	P(B)	k[a]	P(B)	k
$J_- = 0$ at $R = 34.6$ cm	0.8374	1.0377	0.8256	1.0231
$\phi = 0$ at $\tilde{R} = 35$ cm	0.8212	1.0183	0.8044	0.9977
$\phi = 0$ at $\tilde{R} = 36$ cm	0.8297	1.0287	0.8132	1.0086
$\phi = 0$ at $\tilde{R} = 37$ cm	0.8375	1.0384	0.8216	1.0189
$\phi = 0$ at $\tilde{R} = 38$ cm	0.8449	1.0475	0.8294	1.0286

a. The calculation was for $\tilde{R} = R + d = 34.6 + d$ cm and for the fuel solution composed of U^{235} and H_2O only.

EXPERIMENTAL RESULTS

Critical Experiments

The critical systems from which data were obtained in these experiments consisted of aqueous solutions of uranyl nitrate enriched in either the U^{233} or the U^{235} isotope. A 27-1/2-in.-dia aluminum sphere was made critical with both unpoisoned and several poisoned solutions of both isotopes. The neutron poison employed was boric acid. A 48-in.-dia aluminum sphere was used only with unpoisoned solutions of U^{233} and U^{235}. A 5-ft-dia stainless steel cylinder, a diameter chosen to minimize the buckling for the available amount of U^{233}, was made critical at several heights with both U^{233} and U^{235}. The concluding experiments were performed with U^{235} solutions in a 9-ft-dia steel cylinder. At the maximum critical height in this container the neutron leakage was less than 2%, thus limiting the uncertainty in the value of $\bar{\eta}(U^{235})$ to that resulting from the errors in the cross sections. Descriptions of apparatus and experimental details are given in Appendix A.

Buckling Measurements and Extrapolation Distances

Flux traverses with miniature U^{235} fission counters (described in Appendix A) were made in most of the critical geometries to determine the buckling for that geometry. The normalized counter data were fitted to the form

$$y = \frac{A_\phi \sin B_r(x + x_o)}{B_r(x + x_o)}$$

for spheres, and to the forms

$$y = A_\phi \cos B_h(x + x_o) \text{ and}$$

$$y = A_\phi J_o \left[B_r(x + x_o)\right]$$

for the height and radius, respectively, of cylinders.

A preliminary analysis[9] of some of these data has reported values of the extrapolation distances for spheres of 1.9 and 1.0 cm. However, it is now believed that these small values were the result of non-ideal experimental conditions. Since it was necessary to vary the solution height to maintain criticality as the counter was traversed through the sphere, the solution did not fill the sphere when data were taken in the upper half. The void was greater in the 48-in.-dia sphere, for which d was reported as 1.0 cm. The data from these traverses are not valid, even though there were no observable distortions from the expected form of the spatial flux distributions. Values of the extrapolation distances for the spheres have been extrapolated from those obtained from cylinder experiments.

Tables 3 and 4 summarize the buckling values derived from counter traverses in cylindrical systems. Counting data taken within 2 in. of the boundary were excluded from the analyses. The quoted errors are derived from the variances calculated by the IBM-704 in the curve fitting of the experimental data. A number of flux traverses were also analyzed excluding data at a greater distance from the boundaries, and the derived B values, although slightly different, reflect only errors of measurement and not a variation in curvature with distance from center. Although the counting errors in any particular traverse show no difference between different-sized systems, the measurements in the 5-ft-dia cylinder were internally more consistent than those made in the 9-ft-dia cylinder. It is believed that inaccuracies in height measurements in the latter cylinder are responsible. When the extrapolation distances are plotted for different critical heights, a variation greater than their errors is noted. However, it is only for the 69.2-cm-dia sphere and the short cylinders that this variation of d, $\sim$ 0.8 cm, can affect the nonleakage probability by as much as 0.5%. Figure 2 shows this variation.

The extrapolation distances measured with fast-neutron detectors showed no variation beyond the experimental error with critical height, the average value being 3.02 ± 0.28 cm. The average value of the epithermal extrapolation distance, measured with cadmium-covered U^{235} detectors, was 2.97 ± 0.10 cm. Fast and epithermal measurements were made at critical heights of 18 and 41 in. in the 5-ft-dia cylinder.

The apparent difference between the thermal and fast extrapolation distances experimentally observed was similarly evident in the Corn Pone calculations for the 69.2-cm-dia sphere previously discussed.

The experimental bucklings and their pertinence to the nonleakage probability measurements and calculations are further discussed later in this report.

Cross Sections Needed for Calculations

Since the thermal utilization depends upon the absorption cross sections employed, it is appropriate to consider the values used in this report. The continued improvement in methods and techniques of measurement during the past decade has brought recent values of the total cross section of U^{235} from various laboratories into close agreement and the latest tabulation has been used.[10,11,12,13] The fission cross sections, needed only for calculation of corrections, were essentially the older values.[13]

The g-factor for U^{235}, used to obtain the Maxwellian-average value of the cross sections from the 2200 m/sec values, was taken from Westcott and Roy.[12] Since the recent tabulation[15] shows the absorption and fission cross section of U^{233} to be 1/v in the thermal region, the g-factors for these cross sections must be unity. Table 5 shows the cross sections used and the appropriate g-factors.

Table 3. Buckling Measurements in the 60.92 in. Diameter Cylinder

Detector	Solution Height[a] (in.)	(Axial Buckling)$^{1/2}$ B_h (in.$^{-1}$)	Extrapolated Height h (in.)	2d (in.)	Extrapolation Distance d (cm)	B_h^2 (cm^{-2})
U^{235}	18 08	0.1588 ± 0 0006	19.78 ± 0.07	1 70	2.16 ± 0.09	3.909 x 10^{-3}
"	17.91	0.1588 ± 0.0005	19 78 ± 0.05	1.87	2.37 ± 0.07	3.909
"	19.08	0 1495 ± 0.0006	21.01 ± 0.08	1.93	2.45 ± 0.10	3 464
U^{235} + Cd	19.11	0.1474 ± 0.0005	21.31 ± 0.07	2 30	2.92 ± 0.09	3.367
U^{238}	19 01	0.1469 ± 0 0007	21.39 ± 0.10	2.38	3.02 ± 0.13	3.344
U^{235}	28.81	0.1023 ± 0.00025	30 70 ± 0.08	1.89	2.40 ± 0.10	1.623
"	42.07	0.0743 ± 0.00012	44.17 ± 0.07	2.10	2.67 ± 0.09	0.784
U^{235} + Cd	42.30[b] Min	0.07031 ± 0.00015	44.68 ± 0.09	2 38	3 02 ± 0.11	0.766
	42.55[b] Max			2.13	2.71 ± 0.11	
U^{238}	42.35[b] Min	0.07023 ± 0.00045	44.74 ± 0.29	2.39	3 04 ± 0.37	0.764
	42.38[b] Max			2.36	3.00 ± 0.37	
U^{235}	80.12	0.03805 ± 0.00011	82.57 ± 0.24	2.45	3.11 ± 0.30	0.224

Detector	Height (in)	(Radial Buckling)$^{1/2}$ B_r (in.$^{-1}$)	Extrapolated Radius R (in.)	d + ΔR[c] (in.)	d (cm)	B_r^2 (cm^{-2})
U^{235}	41	0 07547 ± 0.00020	31.87 ± 0.08	1.43	3.30 ± 0.20	0.883 x 10^{-3}
U^{238}	41	0 07546 ± 0.00034	31.87 ± 0.14	1.43	3.30 ± 0.36	0.883
U^{235}	80	0.07578 ± 0.00018	31 74 ± 0.08	1.28	2.92 ± 0.20	0.890

a Height measurements have been corrected for dished bottom (0.25 in.) and for bottom reflector (0.53 in.).
b. Height was varied in order to maintain criticality, the maximum occuring while counter was at center.
c. The correction, Δ R, for the container was assumed to be the wall thickness, 0.13 in.

Table 4. Buckling Measurements in the 107.7 in. Diameter Cylinder

Detector	Solution Height[a] (in)	(Axial Buckling)$^{1/2}$ B_h (in $^{-1}$)	Extrapolated Height h (in.)	$h - h_c$ (in)	B_h^2 (cm^{-2})
Gold	35.78	0.08065 ± 0 00017	38.95	3.17 ± 0.08	1.008 x 10^{-3}
U^{235}	35.78	0.08110 ± 0.00023	38.74	2.96 ± 0.11	1 020
"	35.78	0.08118 ± 0.00038	38 70	2.92 ± 0 18	1 021
"	35.68	0.08132 ± 0.00018	38 63	2.95 ± 0.08	1.025
"	91.43	0.03310 ± 0.00005	94 91	3 48 ± 0.14	0.170
"	48 47	0.06248 ± 0.00023	50.28	1.81 ± 0 19	0.605
"	48.54	0.06184 ± 0 00025	50 80	2.26 ± 0.20	0 592
"	35.80	0.08327 ± 0.0002	37.73	1.93 ± 0.09	1.075

Detector	Solution Height	(Radial Buckling)$^{1/2}$ B_r	Extrapolated Radius R	$R - R_c$	B_r^2
U^{235}	35 78	0.04314 ± 0.00012	55.75	1.90 ± 0.15	0.288
"	91.59	0.04312 ± 0.00018	55.77	1.92 ± 0.11	0.288

a. The values of the solution dimensions have not been corrected for effects due to structure surrounding the critical cylinder of solution. The difference in column 5 is, therefore, not exactly proportional to the extrapolation distance

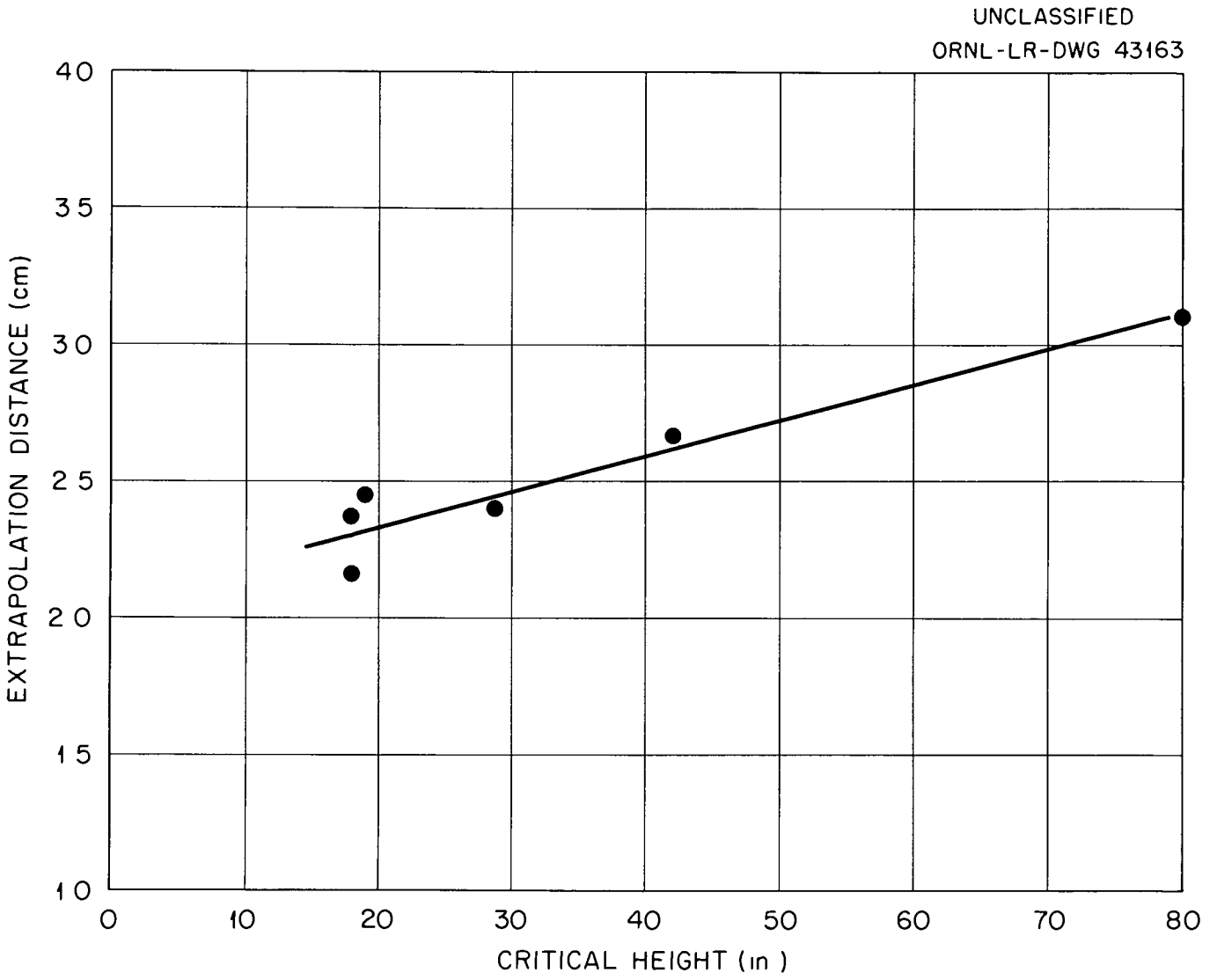

Fig 2 Extrapolation Distances Determined with U^{235} Counter Traverses in 60 92-in -dia Cylinder

Table 5. 2200 m/sec Cross Sections

Isotope	σ_a, (b)	g_a	σ_f, (b)	g_f
U^{233}	577 ± 4	1.0000	527	1.0000
U^{235}	682 ± 3	0.9749	580	0.9754

For the fissile isotopes U^{233} and U^{235}, the resonance integrals given in Table 6 were obtained by numerical machine integration of BNL-325[13,14] curves.

Table 6. Uranium Resonance Integrals

	U^{233}	U^{235}
$\int_{0.2}^{10^6} \frac{\sigma_f}{E} dE$, (b)	930	428
$\int_{0.4}^{10^6} \frac{\sigma_f}{E} dE$, (b)	802	330
$\int_{0.2}^{10^6} \frac{\sigma_t}{E} dE$, (b)	1368	780
$\int_{0.2}^{10^6} \frac{\sigma_a}{E} dE$[a], (b)	1224	636

a. Assuming σ_s = 11 b for the epithermal neutrons.

The following 2200 m/sec microscopic absorption cross sections, assumed to be proportional to 1/v, were used for the other components: hydrogen, 0.332 b; boron, 755 b; nitrogen, 1.88 b; thorium, 7.0 b; U^{238}, 2,75 b;[13] and U^{234}, 113 b;[15] other consitutents contributed negligibly.

Foil Measurements of the Epithermal Flux

The assumption that the flux can be represented by a Maxwellian, ϕ_M, and a λ/E epithermal flux has been discussed previously, and the measurements are

thus dependent on this model. The cadmium ratio, CR, which is the ratio of the activations of bare and cadmium-covered foils, is given by the following equation:

$$CR = \frac{A_{bare}}{A_{cd}} = \frac{\int_0^{\infty} \phi_M \Sigma_{act}\, dE + \int_{0.2}^{10^6} \frac{\lambda}{E} \Sigma_{act}\, dE}{\int_{0.4}^{10^6} \frac{\lambda}{E} \Sigma_{act}\, dE}$$

The cadmium cutoff energy is chosen to be 0.4 ev. This relation assumes no flux depressions or self-shielding effects in the foil activities. For the actual U^{235} foils used, the self-shielding and flux depression effects in the resonance as well as in the thermal range must be included.

Trubey[16] has calculated the self-shielding coefficient for thermal neutrons in the U^{235} metal foils used in these experiments to be 0.79. The flux-weighted average of this factor for the absorptions in resonances was 0.94. The cross sections used in the calculations have been listed previously in Table 5. Attempts were made to measure the order of magnitude of these effects by using foils of different thicknesses and extrapolating to zero thickness. The results of these activations define a flux depression and foil self-shielding factor, based only on bare activations, of 0.76. This agreement with the calculation may, however, be somewhat fortuitous, considering the nature of the measurements and the approximations in the calculations.

Table 7 and Fig. 3 summarize the foil measurements and calculations for the determination of the epithermal flux. The metal and oxide foil measurements, as well as the counter values for both U^{233} and U^{235} detectors in both U^{233} and U^{235} solutions, are included in these data. The foils and their use are described in Appendix B.

The best-fit line through the measurements is $\lambda = 0.682\ \Sigma_{at}$. From the tabulated values of $\xi \Sigma_t$ for various energies,[17] the theoretical expression for λ in infinite systems with no absorption becomes $0.576\ \Sigma_{at}$ at 0.278 ev and has increased to $0.656\ \Sigma_{at}$ at 10.16 ev. This higher value is then constant up to the kilovolt energy region. An average value of λ, weighted by the U^{235} fission cross section in a 1/E spectrum, is $0.63\ \Sigma_{at}$. It is realized that λ is a function of the buckling as well as Σ_{at} in a detailed neutron balance theory, but this correction is small and only adds some scatter to the plot of the data in Fig. 3.

Experimental Determination of Nonleakage Probabilities

The results from the perturbation measurements of the reactivity as a function of solution height can be described in several ways, each

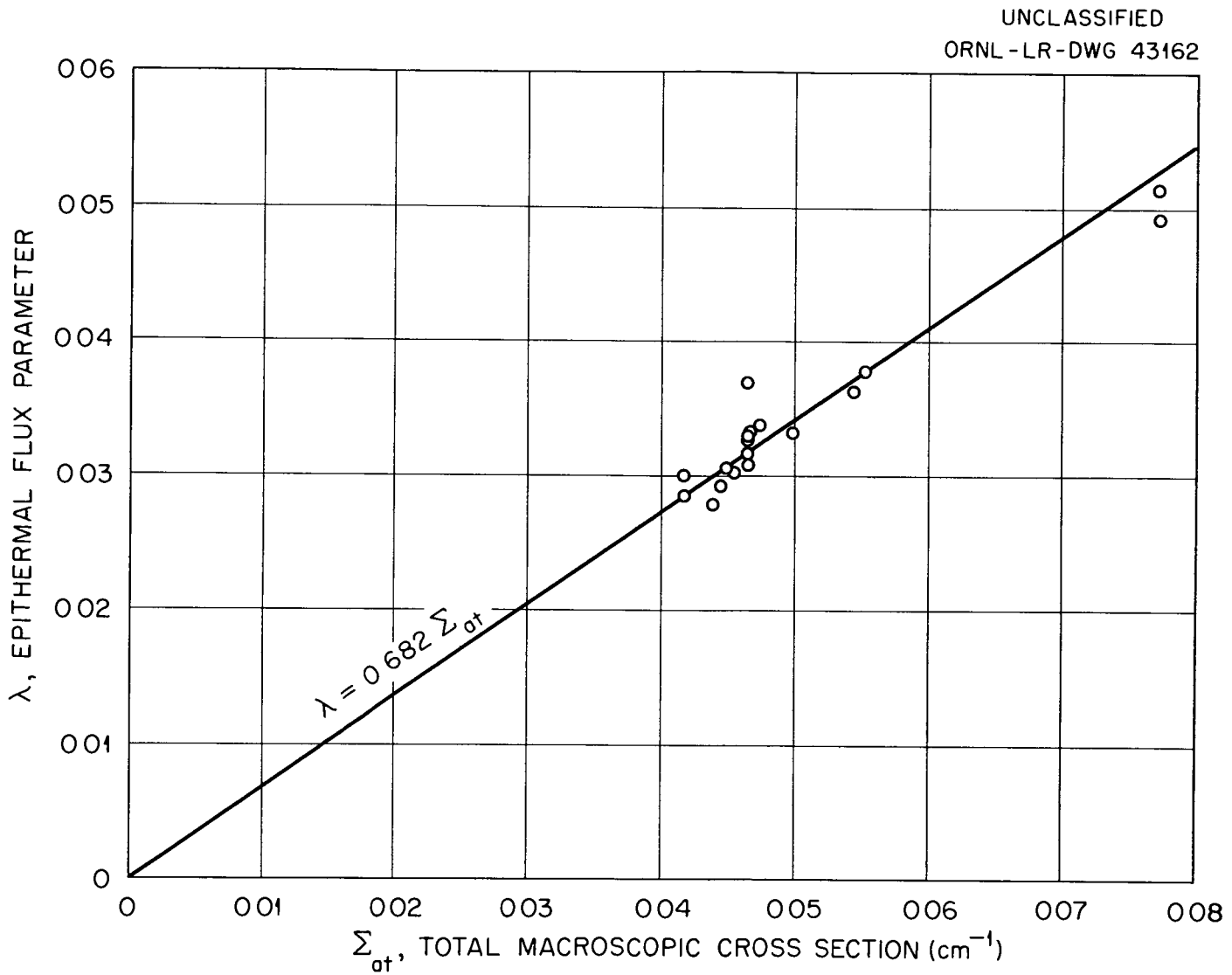

Fig 3 Epithermal Flux Parameter

Table 7. Experimental Determination of λ, the Epithermal Flux Parameter

Solution						
Isotope	Height (in.)	Σ_{at} (cm^{-1})	Detector	Detector Position in Container	Observed Cadmium Ratio	λ [a]
			27.24-in.-dia Aluminum Sphere			
U^{235}	Full	0.05427	U^{235} metal foil	Center	36.50	0.0363
U^{235} + B	"	0.07723	"	"	27.27	0.0492
U^{235} + B	"	"	"	8 in. from center	26.18	0.0514
U^{233}	"	0.04743	"	Center	39.06	0.0338
U^{233} + B	"	0.05523	"	"	36.10	0.0378
			48.04-in.-dia Aluminum Sphere			
U^{235}	Full	0.04629	U^{235} metal foil	Center	42.64	0.0309
"	"	"	$U^{235}O_2$ foil	"	41.55	0.0317
"	"	"	$U^{233}O_2$ foil	"	16.25	0.0328
"	"	"	U^{235} metal foil	18 in. from center	40.00	0.0330
"	"	"	U^{235} counter	Center	49.26	0.0317
"	"	"	U^{233} counter	"	17.08	0.0370
U^{233}	"	0.04166	U^{235} metal foil	"	46.08	0.0285
"	"	"	$U^{233}O_2$ foil	"	17.73	0.0299
			60.92-in.-dia Stainless Steel Cylinder			
U^{235}	17-1/2	0.04975	U^{235} metal foil	Center	39.70	0.0333
"	28	0.04648	"	"	39.67	0.0333
"	41	0.04542	"	"	43.65	0.0302
			107.7-in.-dia Stainless Steel Cylinder			
U^{235}	35	0.04485	U^{235} metal foil	Center	43.05	0.0306
"	47-1/2	0.04430	"	"	44.88	0.0293
"	95	0.04378	"	"	45.45	0.0289

a. Self-shielding and flux-depression factors of 0.79 for thermal neutrons and 0.94 for epithermal neutrons were used for the foils. These factors were assumed to be unity for the counter data.

emphasizing a particular facet of the theoretical model previously discussed. The leakage parameter S, defined in Eqs. 21-22, depends only on the periods resulting from changes in the height after criticality has been established and on the buckling of the critical system. In Fig. 4 this parameter is plotted as a function of buckling for nine measurements in the 5-ft-dia cylinder with both U^{233} and U^{235} solutions and for three measurements in the 9-ft-dia cylinder with U^{235} solutions. Experimentally determined bucklings from U^{235} counter traverses were used for the calculations of ΔB^2. The curves are theoretical values of S based on the equation and parameters shown on the figure.

The variation of L^2, the square of the thermal diffusion length, as a function of buckling, B^2, is shown in Fig. 5 for both U^{233} and U^{235} solutions. The values of L^2 were calculated from the relation

$$L^2 = L_0^2(H_2O) \quad \frac{\Sigma_a(H_2O)}{\Sigma_a(\text{Solution})} ,$$

in which $L_0^2(H_2O) = 7.344\ cm^2$ (Ref. 18).

Since the fast-neutron extrapolation distances measured with U^{238} counters at two critical heights were not significantly different, a constant value, d = 3.0 cm, was used in a second calculation of the parameter S. These values are plotted as a function of buckling as Fig. 6, and the results of both calculations are summarized in Table 8. The curves on Fig. 6 are the same theoretical values of S shown on Fig. 4. As B^2 goes to zero the effect of the extrapolation distance vanishes, thus an extrapolation of either curve to $B^2 = 0$ should give the same value of M^2.

The equation

$$\frac{\partial P(B)}{\partial B^2} = P_d(B) \quad \frac{\sum_i \frac{\beta_i}{1 + \lambda_i T}}{\Delta B^2} = - P_d(B)\ S(B)$$

in which $P_d(B) = \dfrac{1}{1 + \tau_d B^2}$ and $\tau_d = 9\ cm^2$ (Ref. 19)

was used with the Taylor's expansion of P(B) in order to evaluate P(B). This expansion was given in Eq. 20. The correction term, A, was computed by using the theoretical value of τ, 26.5 cm^2, and the values of B^2 and L^2 from each experimental determination. From these values of P(B) experimental ages were computed from the two-group equation, Eq. 19. Figure 7 plots the experimental age as a function of the buckling determined by the U^{235} counter, while Fig. 8 shows the experimental age as a function of the buckling determined by a constant extrapolation distance. For the 9-ft-dia cylinder, only the buckling measured with the U^{235} counters were used in

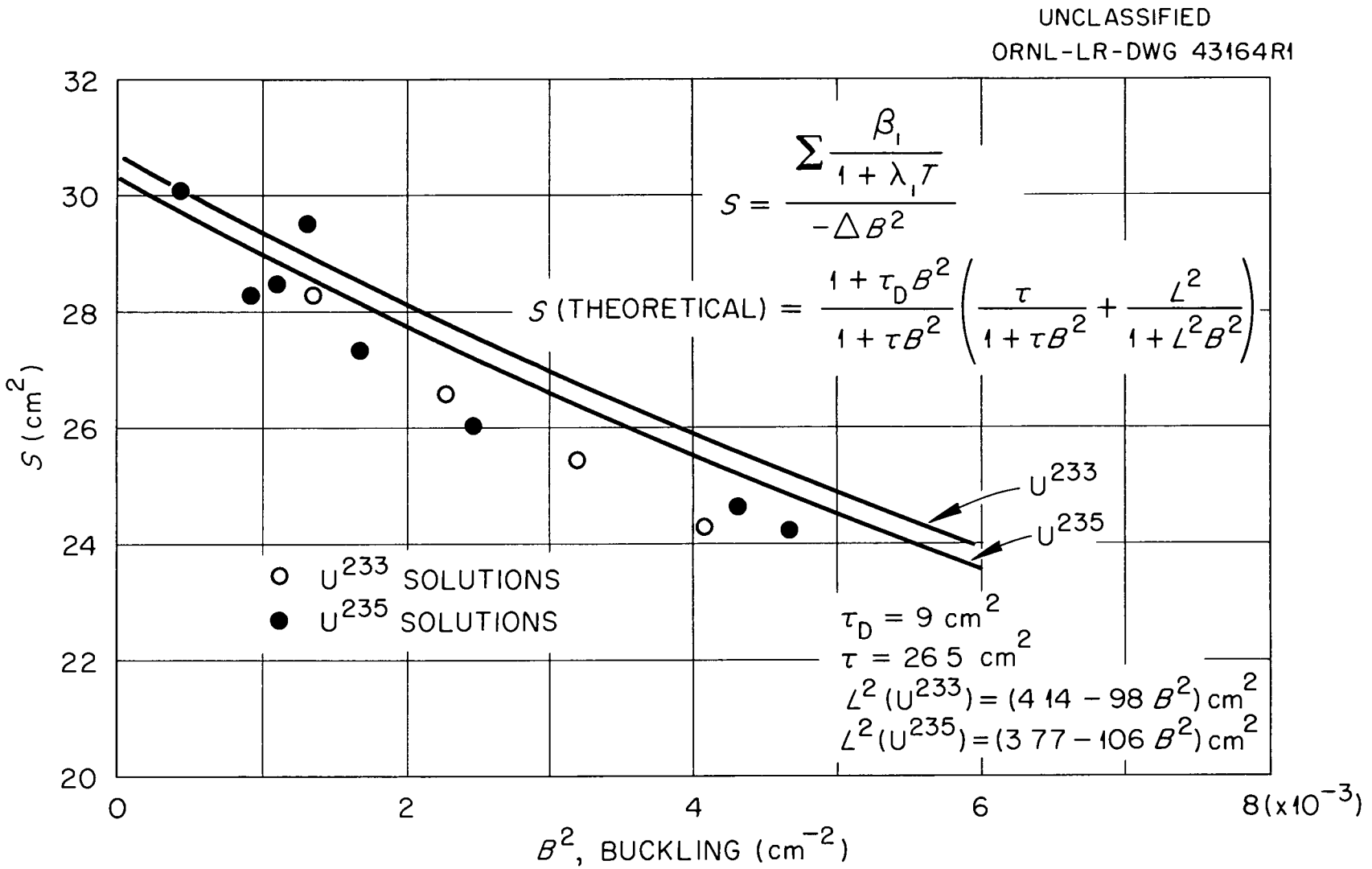

Fig 4 Leakage Parameter Variation with Buckling Determined by the U^{235} Counter

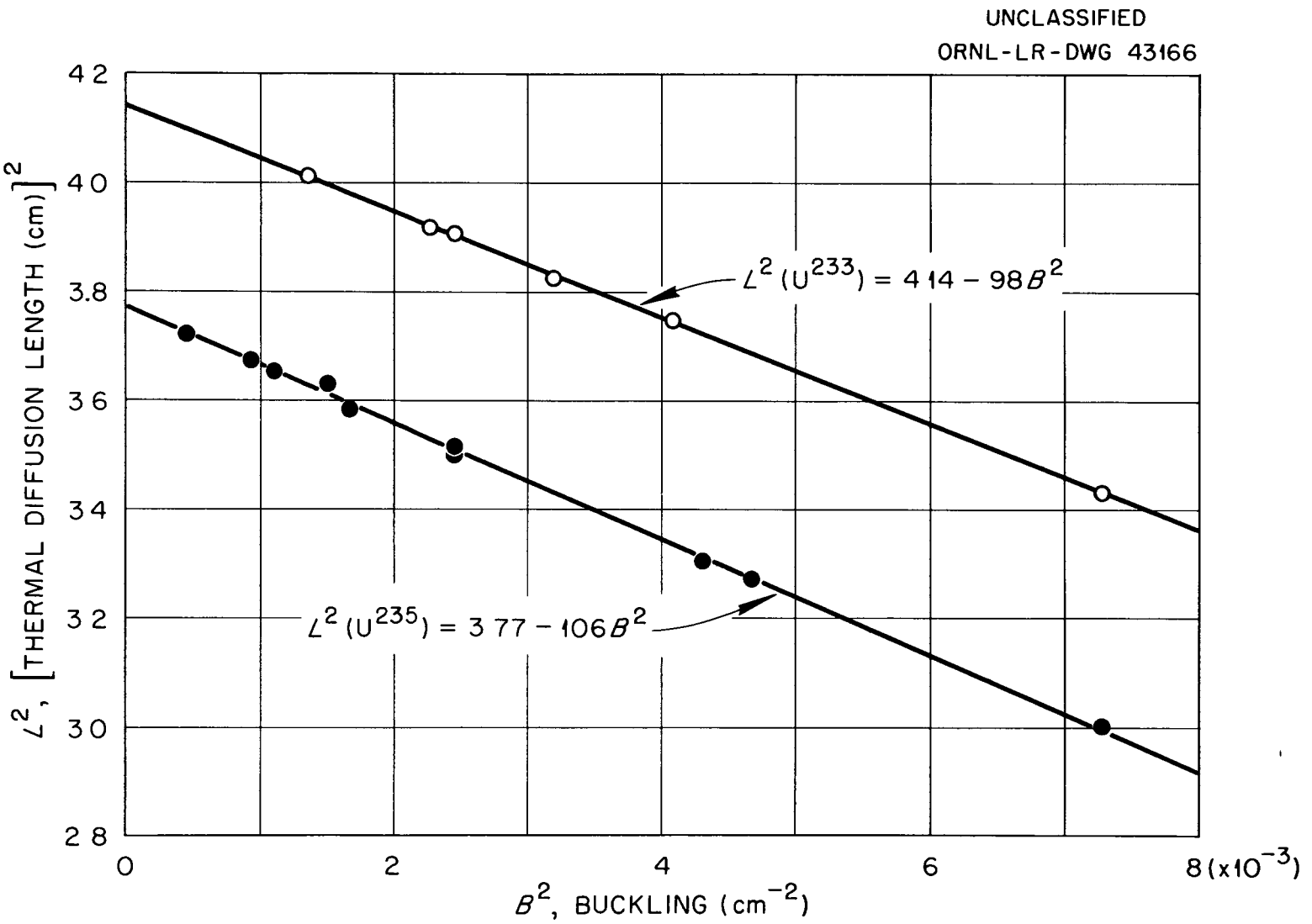

Fig 5 Thermal Diffusion Length

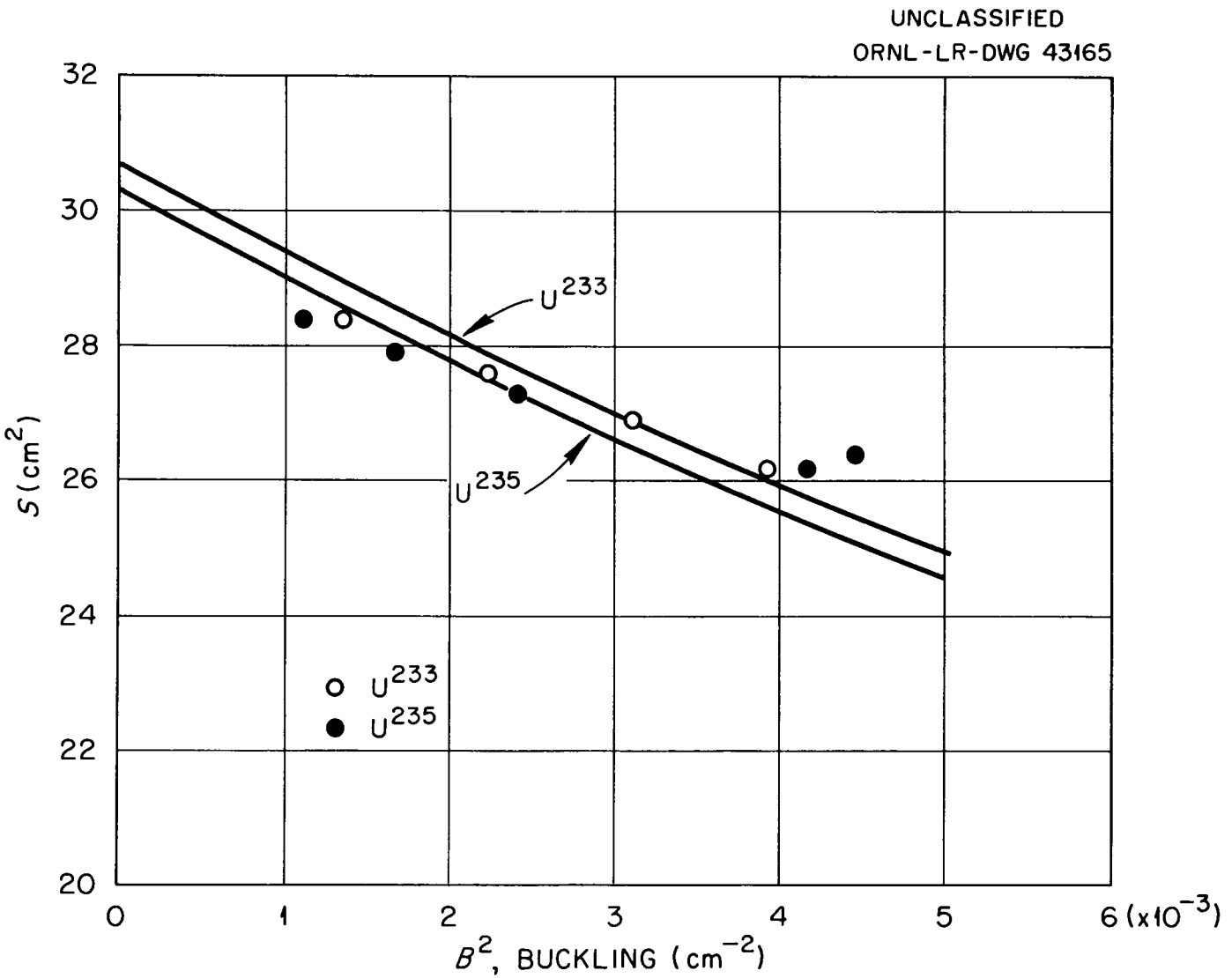

Fig 6. Leakage Parameter Variation with Bucklings Determined by Using $d = 3.0$ cm

Table 8. Summary of Calculations of the Nonleakage Probability and the Age for Cylindrical Geometry

Uranium Isotope	Cylinder Diameter (in.)	Critical Height (in.)	Extrapolation Distance d (cm)	Buckling[a] B^2 (cm^{-2})	S (cm^2)	Calculated[b] Nonleakage Probability	Experimental Nonleakage Probability	Age to Thermal (cm^2)
U^{235}	60.92	17.78	2.27	4.67 ± 0.11	24.3 ± 0.9	0.8764	0.8814 ± 0.0075	25.1
			3.00	4.46	26.4	0.8814	0.8759	28.1
U^{235}	60.92	18.67	2.45	4.31 ± 0.10	24.7 ± 0.9	0.8850	0.8880 ± 0.0069	25.6
			3.00	4.17	26.2	0.8883	0.8854	27.4
U^{235}	60.92	28.70	2.40	2.47 ± 0.05	26.1 ± 0.6	0.9307	0.9340 ± 0.0035	25.0
			3.00	2.42	27.3	0.9319	0.9320	26.4
U^{235}	60.92	41.53	2.67	1.67 ± 0.03	27.3 ± 0.5	0.9518	0.9534 ± 0.0023	25.5
			3.00	1.66	27.9	0.9521	0.9528	26.1
U^{235}	60.92	80.15	3.11	1.11 ± 0.02	28.5 ± 0.3	0.9677	0.9680 ± 0.0014	26.1
			3.00	1.10	28.4	0.9678	0.9683	26.0
U^{233}	60.92	19.41	2.60	4.09 ± 0.10	24.3 ± 0.8	0.8885	0.8967 ± 0.0064	24.0
			3.00	3.93	26.2	0.8926	0.8927	26.5
U^{233}	60.92	23.32	2.65	3.20 ± 0.07	25.4 ± 0.7	0.9108	0.9160 ± 0.0053	24.6
			3.00	3.11	26.9	0.9130	0.9132	26.4
U^{233}	60.92	30.59	2.72	2.29 ± 0.05	26.6 ± 0.6	0.9346	0.9378 ± 0.0033	24.9
			3.00	2.25	27.6	0.9355	0.9362	26.1
U^{233}	60.92	54.65	3.04	1.35 ± 0.03	28.3 ± 0.5	0.9603	0.9612 ± 0.0019	25.8
			3.00	1.35	28.4	0.9602	0.9610	25.9
U^{235}	107.7	39.2		1.31 ± 0.02	29.5 ± 0.6	0.9618	0.9606 ± 0.0020	27.5
U^{235}	107.7	47.5		0.93 ± 0.01	28.3 ± 0.5	0.9727	0.9767 ± 0.0013	25.7
U^{235}	107.7	95.5		0.44 ± 0.01	30.1 ± 0.3	0.9869	0.9883 ± 0.0006	27.0

$\tau_{th} = 25.6 \pm 0.3$

$\tau_f = 26.5 \pm 0.2$

Average $\tau = 26.0 \pm 0.2$

a. Two extrapolation distances and two bucklings are given for each system, the first determined from U^{235} counter flux traverses, the second from U^{238} counter traverses. For the 9-ft-dia cylinder experiments, only U^{235} counter traverses were made to determine the buckling. Critical heights have been corrected by 0.53 in. from bottom reflector savings for calculation of d in the 60.92-in.-dia cylinder.

b. Calculated from the equation $P(B) = [(1 + \tau B^2)(1 + L^2B^2)]^{-1}$ with $\tau = 26.5$ cm^2.

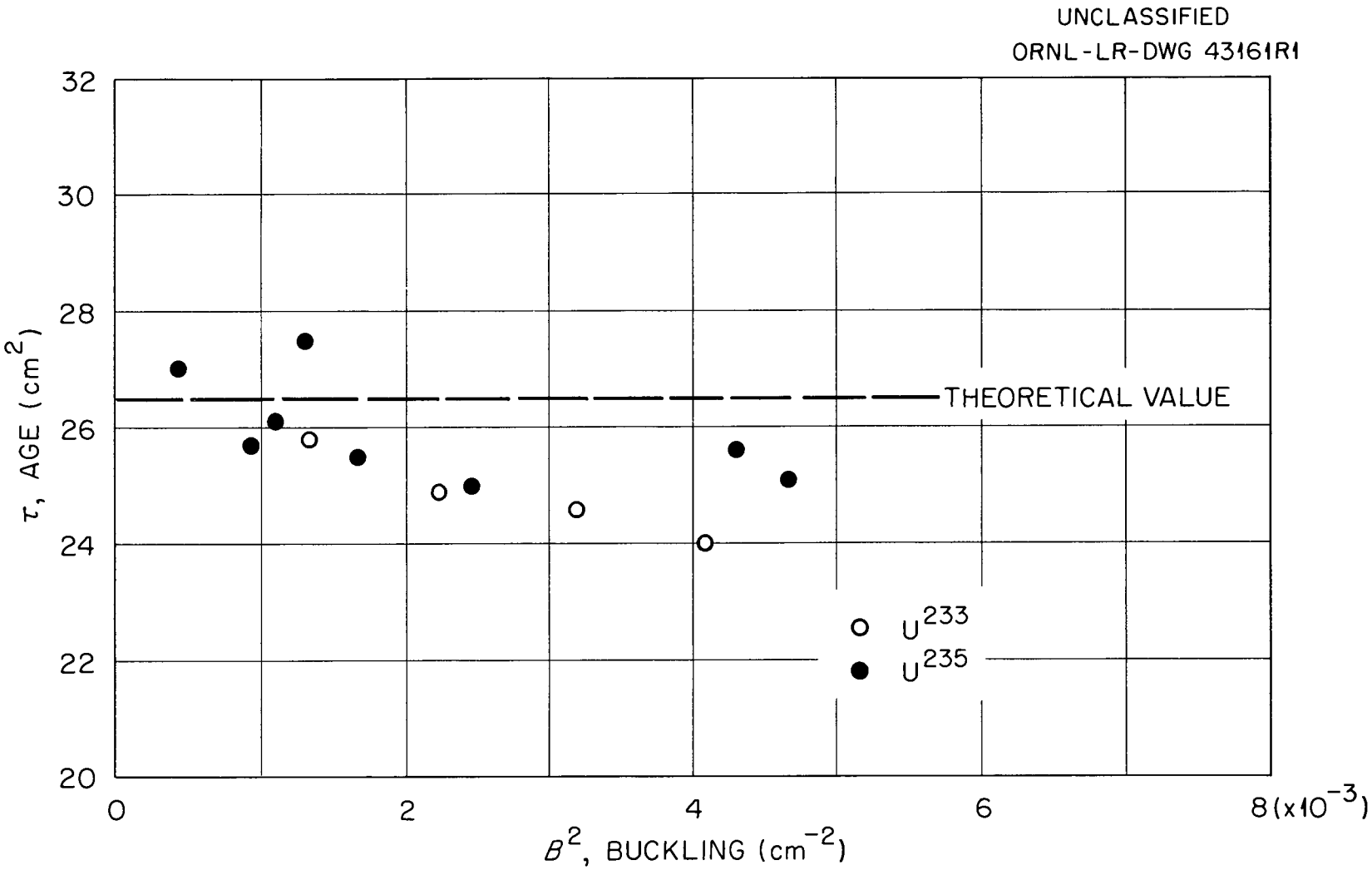

Fig 7. Age to Thermal, Using Bucklings Determined with U^{235} Counter

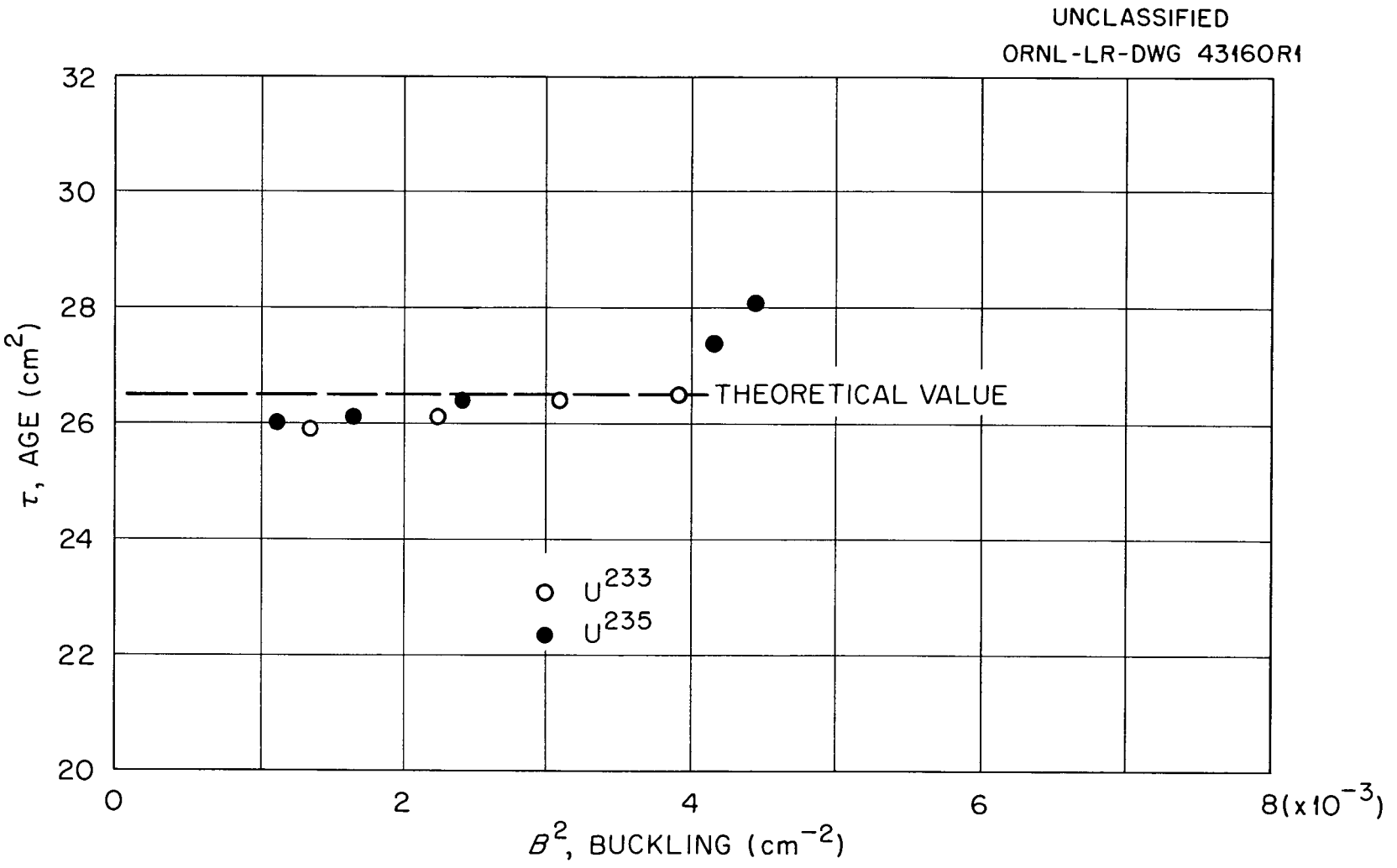

Fig 8. Age to Thermal, Using Bucklings Determined by a Constant Extrapolation Distance

the age calculations. It is seen that the age based on a constant extrapolation distance, derived from bucklings measured with bare U^{238} or cadmium-covered U^{235} counters, 26.5 ± 0.2 cm, is in better agreement with the theoretical age, 26.5 cm, than the age based on thermal bucklings, 25.6 ± 0.3 cm. Because of the quoted uncertainty of 4% in the absolute yield of delayed neutrons,[20] the error in the age must be increased to ± 1.4 cm^2. It is concluded that, within the precision of these experiments and accuracy of the delayed neutron fractions, the ages of fission neutrons from U^{233} and U^{235} are the same.

The measured reactivities have been based on delayed neutron data[20] in which the value of ν was taken as 2.47. If recent values of ν = 2.420 ± 0.037 or ν = 2.426 ± 0.068 (Ref. 21) are used, then the delayed neutron fraction must be increased by 2%, and the value of S and the experimental ages calculated from the reactivity measurements would also be increased by this percentage. The above values for the age-to-thermal energy become 27.0 and 26.1 cm^2, respectively. The average is then 26.5 ± 1.4 cm^2. The age-to-indium-resonance energy based on the reduced values of ν is 25.5 cm^2, which is identical with the theoretical value computed by Coveyou and Sullivan.[22]

Calculation of Eta from Critical Experiments

The measurement of the nonleakage probability in cylindrical geometry has resulted in confirmation of the theoretical value of the age of fission neutrons to thermal energy. This agreement does not prove that this model can be used for bucklings significantly beyond the range of these experiments. However, such agreement does encourage confidence in the experimental measurements and in the suitability of the model. On this basis, therefore, the sphere comparison measurements have been evaluated also and a value of eta obtained, subject to the errors in epithermal corrections and in the cross sections. It should be emphasized that the eta ratios obtained from the sphere comparisons are not affected by the errors in the nonleakage probability.

All eta values and ratios were calculated with τ = 26.5 cm^2 and the thermal and fast bucklings, and each value was assigned the same statistical weight in computing the average value. The experimental data are given in Tables 9, 10, and 11. The calculations are summarized in Table 12.

The eta ratios, $\bar{\eta}$ of $U^{233}/\bar{\eta}$ of U^{235}, deduced from experiments in individual vessels were:

From 9 experiments in the 27-in.-dia sphere, 1.100;
from 2 experiments in the 48-in.-dia sphere, 1.102; and
from 9 experiments in the 61-in.-dia cylinder, 1.103.

The average thermal values of eta are: $\bar{\eta}(U^{233})$ = 2.284 ± 0.015; $\bar{\eta}(U^{235})$ = 2.074 ± 0.015. The average value of the ratio $\bar{\eta}$ of $U^{233}/\bar{\eta}$ of U^{235} is

Table 9. Experimental Data for Critical Conditions of Spheres

Experiment Number	Isotopic Composition (wt%)					Solution Density (g/ml)	Total Uranium (mg/g)	Total Boron (mg/g)	Total Nitrate (mg/g)	Total Thorium (mg/g)	$(k-1)\times10^4$ at 20°C
	U^{233}	U^{234}	U^{235}	U^{236}	U^{238}						
27.24-in.-dia Aluminum Sphere											
1	0.00	1.04	93.18	0.27	5.51	1.0288	19.56	0.00	18.7	0.00	11.8
2	0.00	1.04	93.18	0.27	5.51	1.0333	22.77	0.0905	21.2	0.00	7.3
3	0.00	1.04	93.18	0.27	5.51	1.0387	25.77	0.18	23.7	0.00	9.0
4	0.00	1.04	93.18	0.27	5.51	1.0445	27.24	0.22	25.1	0.00	2.8
5	97.70	1.62	0.04	0.00	0.64	1.0226	16.76	0.00	11.9	0.074	5.0
6	97.70	1.62	0.04	0.00	0.64	1.0253	17.42	0.0233	12.3	0.077	10.3
7	97.70	1.62	0.04	0.00	0.64	1.0274	18.03	0.0453	12.8	0.080	10.9
8	97.70	1.62	0.04	0.00	0.64	1.0275	18.67	0.0670	13.2	0.083	3.3
9	97.70	1.62	0.04	0.00	0.64	1.0286	19.27	0.0887	13.6	0.085	4.4
48.04-in.-dia Aluminum Sphere											
10	0.01	1.05	93.21	0.54	5.19	1.0216	14.82	0.00	11.3	0.00	12.9
11	97.67	1.54	0.03	0.00	0.76	1.0153	13.05	0.00	7.6	0.056	4.6

Table 10. Experimental Data for Critical Conditions of Cylinders

Experiment Number	Critical Solution Height (in.)	Isotopic Composition (wt%)					Solution Density (g/ml)	Total Uranium (mg/g)	Total Nitrate (mg/g)	Total Thorium (mg/g)
		U^{233}	U^{234}	U^{235}	U^{236}	U^{238}				
60.92-in.-dia Cylinder										
12	17.77	0.00	1.05	93.22	0.55	5.18	1.0229	16.92	12.8	0.00
13	18.68	0.00	1.03	93.03	0.51	5.43	1.0247	16.61	14.2	0.00
14	28.64	0.00	1.04	93.12	0.54	5.30	1.0209	14.96	12.0	0.00
15	41.45	0.00	1.06	93.11	0.52	5.31	1.0204	14.31	12.2	0.00
16	80.06	0.00	1.06	93.01	0.52	5.41	1.0197	13.79	12.6	0.00
17	19.49	97.37	1.50	0.04	0.00	1.09	1.0203	14.21	8.3	0.014
18	23.31	97.35	1.52	0.05	0.00	1.08	1.0198	13.62	8.6	0.012
19	30.58	97.30	1.49	0.05	0.00	1.16	1.0169	13.00	8.1	0.014
20	54.69	97.25	1.55	0.05	0.00	1.16	1.0166	12.33	8.1	0.098
107.7-in.-dia Cylinder										
21	35.8	0.00	1.08	92.79	0.66	5.47	1.0194	14.00	14.2	0.00
22	48.21	0.00	1.06	92.78	0.65	5.51	1.0218	13.66	13.8	0.00
23	94.9	0.00	1.05	92.82	0.63	5.50	1.0210	13.33	13.5	0.00

Table 11 Atom Densities x 10^{-20} for the Critical Experiments (cm^{-3})

Experiment	Solution Height (in)	Uranium Isotope U^{233}	234	235	236	238	N	H	B	H/X
				27 24-in -dia Sphere						
1	Full		0 00538	0 48066	0 00138	0 02807	1 869	662 28		1378
2	"		0 00631	0 56206	0 00163	0 03281	2 129	661 48	0.052	1177
3	"		0 00716	0 63944	0 00184	0 03734	2 392	660 70	0 104	1033
4	"		0 00762	0 67959	0 00197	0 03967	2 548	660 28	0 128	972
5	"	0 43284	0 00716	0 00018		0 00281	1 178	663 60		1533
6	"	0 45120	0 00744	0 00018		0 00291	1 224	663 45	0.0133	1470
7	"	0 46798	0 00772	0 00018		0 00301	1 274	663 29	0 0259	1417
8	"	0 48455	0 00801	0.00021		0 00311	1 319	663 15	0.0383	1368
9	"	0 05066	0.00827	0 00021		0 00327	1 363	663 00	0 0508	1324
				48 04-in -dia Sphere						
10	Full		0 00409	0.36185	0 00220	0 01985	1 116	663 94		1835
11	"	0.33460	0 00525	0 00010		0 00256	0 753	664 67		1986
				60 92-in -dia Cylinder						
12	17 77		0.00469	0 41364	0 00243	0 02271	1 272	663 45		1604
13	18 68		0 00451	0 40595	0 00222	0 02339	1 409	663.43		1634
14	28 64		0.00409	0 36452	0 00209	0 02048	1 185	663.83		1821
15	41 42		0.00397	0 34845	0 00194	0 01962	1 208	663 89		1905
16	80 03		0 00384	0 33519	0 00186	0.01924	1 244	663 91		1981
17	19 49	0 36517	0 00556			0 00410	0 826	664 39		1819
18	23 31	0 34978	0 00525			0 00395	0 849	664 44		1900
19	30 58	0 33292	0 00507			0 00375	0 802	664 59		1996
20	54 69	0 31567	0 00481			0.00354	0 795	664 70		2106
				107 7-in -dia Cylinder						
21	35 78		0 00397	0 33940	0 00240	0 01975	1 407	663 67		1955
22	48.20		0 00381	0 33124	0 00232	0 01942	1 367	663 74		2004
23	94 93		0 00368	0 32347	0 00220	0 01894	1 338	663 85		2052

Table 12. Critical Experiment Calculations

Experiment Number[a]	f	F	L^2 (cm^2)	B_{th}^2 (cm^{-2})	$P(B_{th})$	$\eta(\tau, B_{th})$	B_F^2 (cm^{-2})	$P(B_F)$	$\bar{\eta}(\tau, B_F)$
				(x10-3)			(x10-3)		
1	0.5878	0 9961	2 999	7 288	0 8202	2 082	6 981	0 8266	2 066
2	0 5863	0.9955	2 557	"	0.8228	2 082	"	0 8290	2.067
3	0 5835	0 9949	2 237	"	0 8247	2 089	"	0 8309	2 073
4	0 5840	0 9946	2 107	"	0 8254	2 086	"	0 8317	2 070
5	0 5280	1 0107	3 431	'	0 8177	2 292	"	0.8241	2 274
6	0 5273	1.0112	3 287	'	0.8185	2 291	"	0 8249	2 273
7	0 5264	1 0116	3 164	"	0 8192	2 292	"	0 8256	2 275
8	0 5254	1 0122	3 045	"	0 8199	2 293	"	0 8263	2 276
9	0 5245	1 0126	2.947	"	0 8205	2 295		0 8269	2 277
10	0 5189	0 9972	3 515	2 455	0 9308	2.076	2 409	0 9321	2 073
11	0 4644	1 0122	3 906	'	0.9300	2 287	"	0 9312	2 284
12	0 5519	0 9967	3 271	4 672	0 8764	2 074	4 46	0 8814	2 063
13	0.5470	0 9968	3 304	4 311	0 8850	2 072	4 17	0 8883	2 065
14	0 5206	0 9971	3 501	2 465	0 9307	2 070	2 42	0 9319	2.067
15	0 5093	0 9973	3 583	1 670	0 9518	2 069	1 66	0 9521	2 068
16	0.4996	0 9975	3 653	1 106	0 9677	2 074	1 10	0 9678	2 073
17	0 4861	1 0117	3 746	4 093	0 8885	2 289	3 93	0 8926	2 278
18	0 4753	1 0120	3 825	3 197	0 9108	2 283	3 11	0 9130	2 277
19	0.4631	1 0122	3 915	2 285	0 9346	2 283	2 25	0 9355	2 280
20	0 4499	1 0126	4 012	1 349	0 9603	2 286	1 35	0 9602	2 286
21	0 5024	0 9973	3 628	1 31	0 9618	2 075			(2 075)[b]
22	0.4964	0 9974	3 673	0 93	0 9727	2 076			(2 076)[b]
23	0 4905	0 9976	3 717	0 44	0 9869	2 071			(2 071)[b]
Averages					$\bar{\eta}(U^{233})$	2 289			2 278
					$\bar{\eta}(U^{235})$	2 077			2 070
					$\bar{\eta}(U^{233})/\bar{\eta}(U^{235})$	1 102			1.100

a See Tables 9 and 10 for identification

b This value of η was assumed to be the same as that calculated using the thermal neutron extrapolation distance since, for this large system, the nonleakage probability and, hence, the calculated η is insensitive to differences in the extrapolation distance

1.101 ± 0.008. These values of eta and the eta ratio are the same as the 2200 m/sec values since the g-factors for eta are unity.

Supplementary Data

From the data primarily obtained for the calculation of η, other information of interest in the fields of reactor physics and nuclear safety can be deduced. The analyses of the critical solutions in spheres and cylinders are given in Tables 9 and 10. If, from these data, the concentration of the fissile isotope is plotted as a function of the thermal bucklings shown in Tables 8 and 11, extrapolation to zero buckling can be made. The intercepts are the limiting critical concentration of U^{233} and U^{235} in these nitrate solutions. This plot is shown as Fig 9. The limiting critical concentrations are 11.25 g/liter for the U^{233} solutions and 12.20 g/liter for the U^{235} solutions.

In addition, if the hydrogen-to-uranium ratio from Table 11 is plotted as a function of the nonleakage probability, the result is a straight line. The intercept at P(B) = 1 then represents the limiting H/X ratio for each of the nitrate solutions used in these experiments. This plot is shown as Fig. 10. The limiting concentrations for these particular nitrate solutions are $H:U^{233}$ = 2260 and $H:U^{235}$ = 2110.

Error Analysis

The error analysis has been based on the experimental deviations of the measured quantities and the quoted errors on all quantities used in the calculations. Since the multiplication factor of a critical system can be determined to less than 1×10^{-4}, the errors in the eta values are compounded only from nonleakage probability errors and thermal utilization errors.

The errors in the nonleakage probabilities are made up of errors in the leakage parameter, S, and the quoted error of 4% in the absolute delayed neutron yield. The errors in the leakage parameter, S, were determined by the observed deviations of reactivities as a function of buckling, B^2, where buckling errors are based on a ± 0.3 cm error in the extrapolation distance. This value was derived from the variance in the least squares fit of the counter data from the measured flux traverses.

Thermal utilization errors are dependent upon the macroscopic cross section errors, and range from 0.4% for small systems to 0.5% in the largest systems. These values are compounded from a 0.5% error in the uranium cross sections, a 0.5% error in the uranium density, and a 0.6% error in the hydrogen cross section.

The errors in the epithermal flux and the resonance integrals can be as large as 10% without introducing more than 0.1% error in the epithermal flux

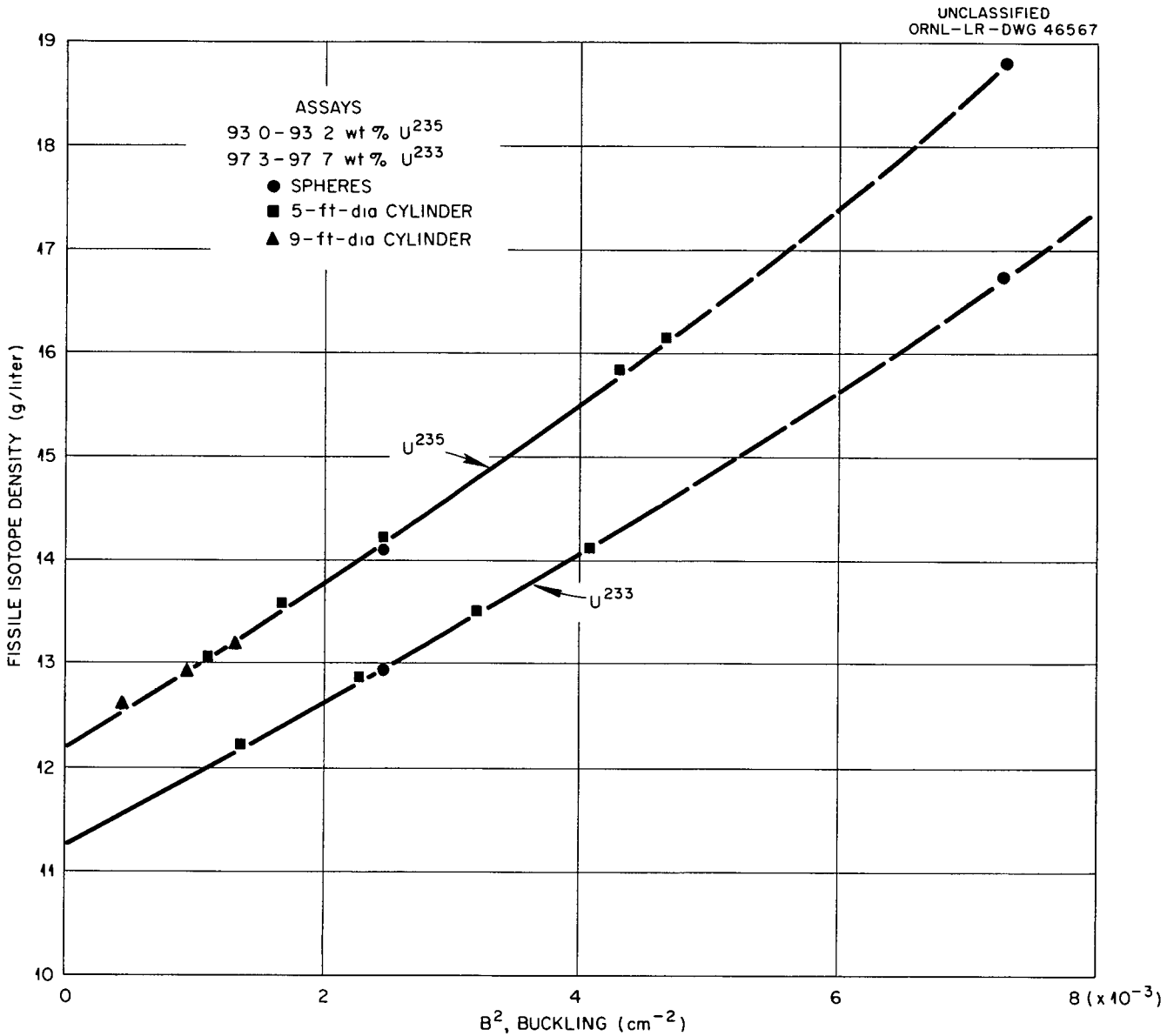

Fig. 9 Fissile Isotope Densities as a Function of Buckling in Critical Aqueous Solutions of the Nitrates of U^{233} and U^{235}

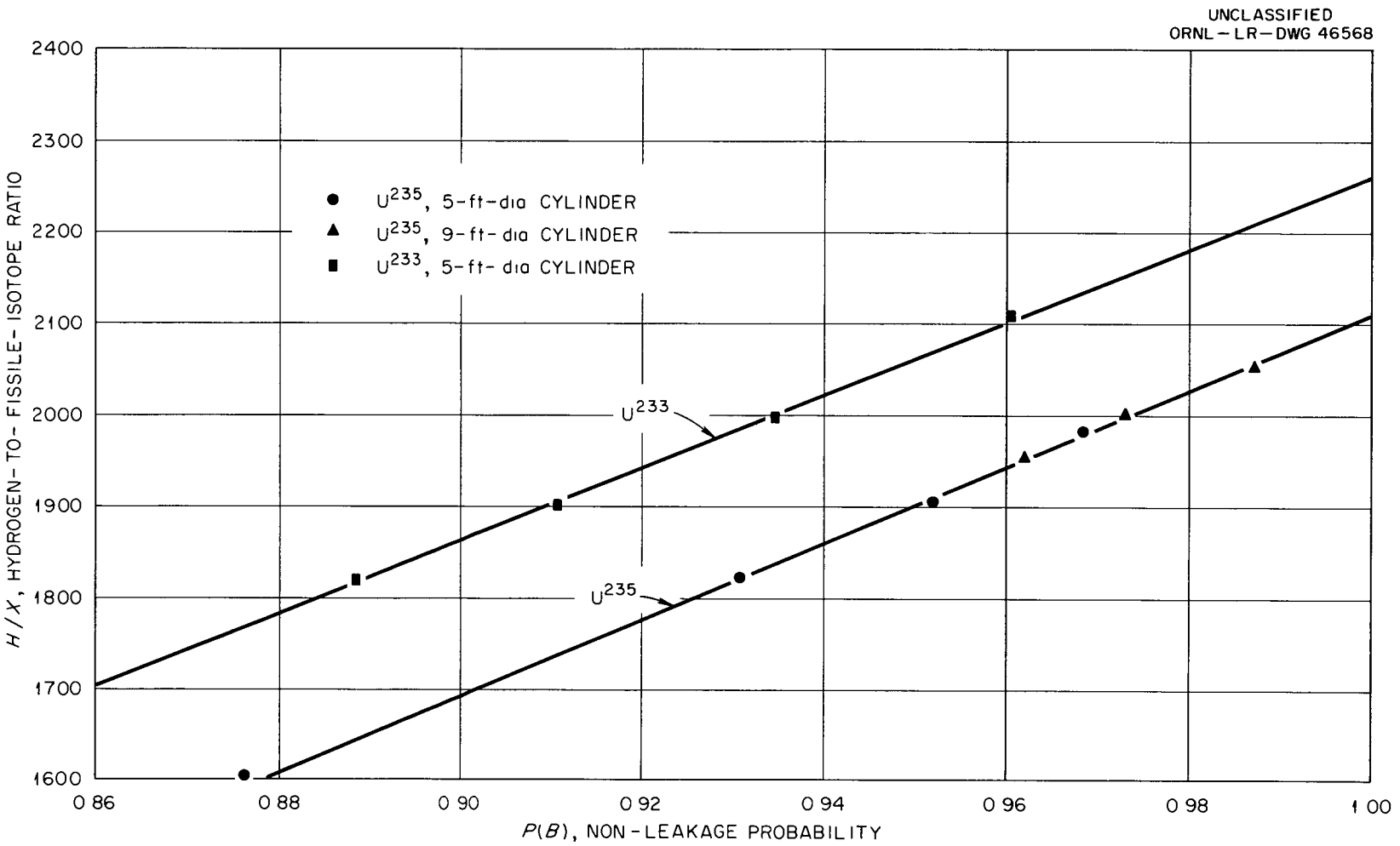

Fig 10 The Hydrogen-to-Fissile-Isotope Ratio as a Function of the Non-Leakage Probability

correction factor. Since the epithermal fissions have been correctly accounted for by using the appropriate isotope in the foil measurements, the only source of error in the correction for epithermal absorptions is in the epithermal captures in the uranium isotopes. In other words, the ratio of the fission and absorption integrals might be in error. Because of the size of the epithermal correction factor, F, only 1% different from unity, no error has been included for this term.

SUMMARY

A series of experiments has been performed to determine the critical conditions of unreflected homogeneous aqueous solutions of the nitrates of U^{233} and U^{235} in both cylindrical and spherical vessels. These critical conditions have been used to calculate the thermal values of η for both isotopes. The average values obtained were: $\bar{\eta}(U^{233}) = 2.284 \pm 0.015$ and $\bar{\eta}(U^{235}) = 2.074 \pm 0.015$. From these values the ratio $\bar{\eta}(U^{233})/\bar{\eta}(U^{235})$ was 1.101 ± 0.008. The ratio $\bar{\eta}(U^{233})/\bar{\eta}(U^{235})$ may also be compared with the value of 1.113 ± 0.018 obtained by the present authors by a reactivity coefficient experiment.[23] These results may be compared to the absolute values at 2200 m/sec as measured by Macklin and deSaussure[24] which are $\eta(U^{233}) = 2.296 \pm 0.010$, $\eta(U^{235}) = 2.077 \pm 0.010$, and $\eta(U^{233})/\eta(U^{235}) = 1.105 \pm 0.007$. This comparison to 2200 m/sec values is valid because the g-factors for eta are unity.

Bucklings were measured in most of the experimental configurations by using miniature U^{235} fission counters. These measurements indicated a variation in extrapolation distance with height of assembly, an assembly 18 in. high having a $d = 2.2 \pm 0.1$ cm, while an 80-in.-high assembly had an extrapolation distance of 3.1 ± 0.3 cm. Measurements of the extrapolation distance with U^{238} or cadmium-covered U^{235} fission chambers did not show a height dependence greater than the experimental error, the value being $d = 3.0 \pm 0.3$ cm.

Nonleakage probability measurements made in cylindrical geometry were found to differ less than 0.3% from calculated values based on a two-group model using the experimentally determined bucklings and the theoretically calculated age of 26.5 cm^2. Inclusion of epithermal absorptions and fissions in the analysis produced small corrections.

From the analysis of the experimental data it is concluded that a consistent theoretical model has been employed. The experiments have demonstrated consistency between the direct measurement of eta, the theoretical age and recent cross section measurements.

ACKNOWLEDGEMENTS

The authors acknowledge the participation of J. K. Fox, L. W. Gilley, and D. F. Cronin in the design and performance of the experiments in the 9-ft-dia cylinder. C. Cross and R. K. Reedy provided much technical assistance in these experiments and their precautions during the U^{233} experiments prevented any radioactive contamination.

The cooperation of D. K. Trubey, W. E. Kinney, L. Dresner, R. R. Coveyou, and J. G. Sullivan contributed much to the interpretation of the experiments.

Appendix A

EXPERIMENTAL DETAILS

Nuclear Instrumentation

Both neutron and gamma-sensitive instruments were used in these experiments. The neutron-sensitive instruments were BF_3-filled ion chambers and proportional counters and miniature fission counters which contained U^{233}, U^{235} and U^{238} films.* The gamma-sensitive instruments were anthracene crystal scintillation detectors. Both types of instruments were used in the safety circuits.

Since the neutron-sensitive instruments were used in reactivity measurements, it is appropriate to describe them in more detail. The enriched and normal BF_3 ion chambers, made at ORNL from the design of Haake,[25] were used with the recorded output of logarithmic amplifiers of several types, including a Beckman, a Keithley, and an ORNL model. The instruments were calibrated several times daily by internal calibrating currents which, in turn, were checked repeatedly against a standard current generator. Periods were derived by alignment of a straightedge on the recorded traces, which were essentially linear over two decades. Timing tests of the chart drives indicated errors less than 0.5%. The power levels were selected so that the chamber output was always below saturation but was at least 2 decades above background. In the U^{233} experiments the chambers were surrounded with lead in order to reduce the effects of the gamma rays arising from decay products of U^{232}, a contaminant of U^{233}. Proportional counters** and miniature fission counters with associated scalers were also used for period determinations. The fission counters, constructed by the ORNL Instrument Department and described in Fig. 11, were utilized for the flux traverses.

27-in.-dia Sphere

Hemispherical shells, spun from Type 1100 sheet aluminum, were welded into a sphere. At the poles of the sphere with respect to the equatorial weld, 2-in.-dia tubes were attached which served for filling and venting. The upper one also served as access port to the sphere for foils and counters. The lower tube was flanged for attachment to the solution handling system. The capacity, 173.6 liters, was measured with volumetric flasks and by weighing the water contained by the sphere. The volume averaged diameter was 27.24 in. To prevent corrosion the interior surfaces of the aluminum vessel were coated with a phenolic-base baked-on enamel which had no appreciable amounts of neutron absorbers. The sphere as installed on the support platform is shown in Fig. 12. The storage vessel, pump, and piping, made of stainless steel, are located below the support stand.

---

* The U^{238} and some of the U^{235} films were prepared by C. A. Kienberger at ORGDP; the other films were prepared by G. A. Jarvis of LASL.

** Both RCL-10500 and RCL-10502 BF_3 proportional counters were used.

UNCLASSIFIED
ORNL-LR-DWG 45676

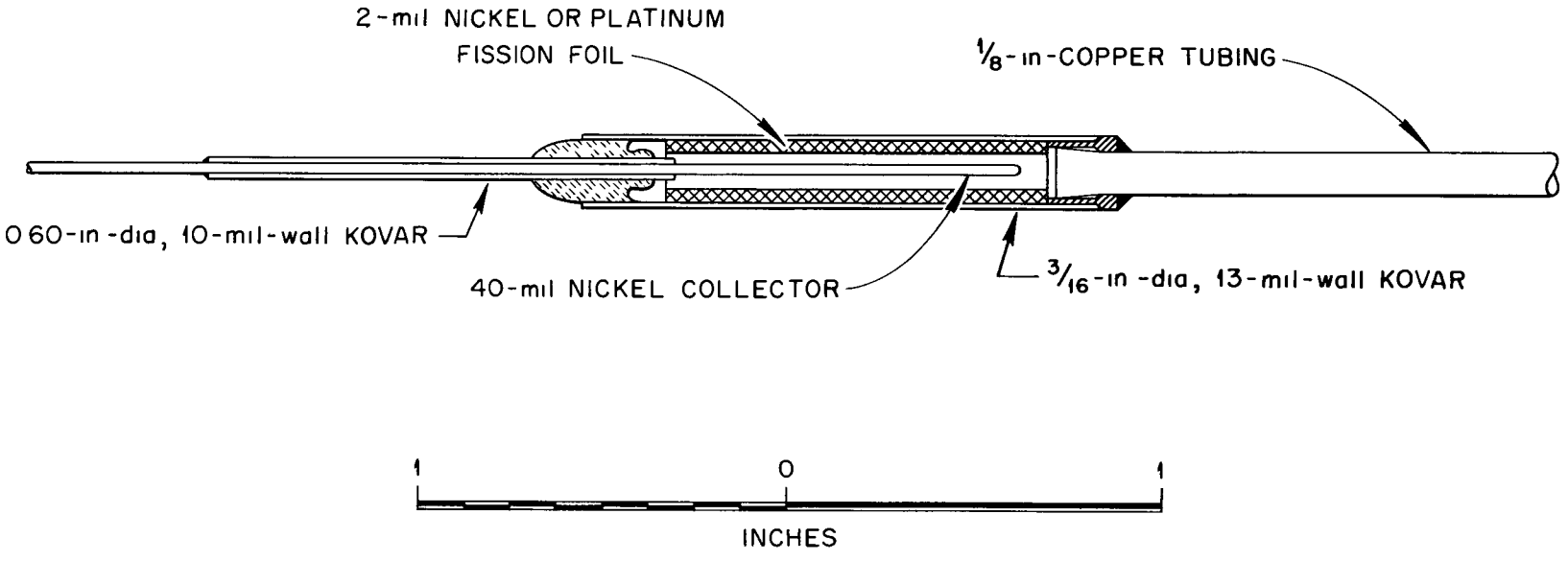

Fig 11 Miniature Fission Chamber.

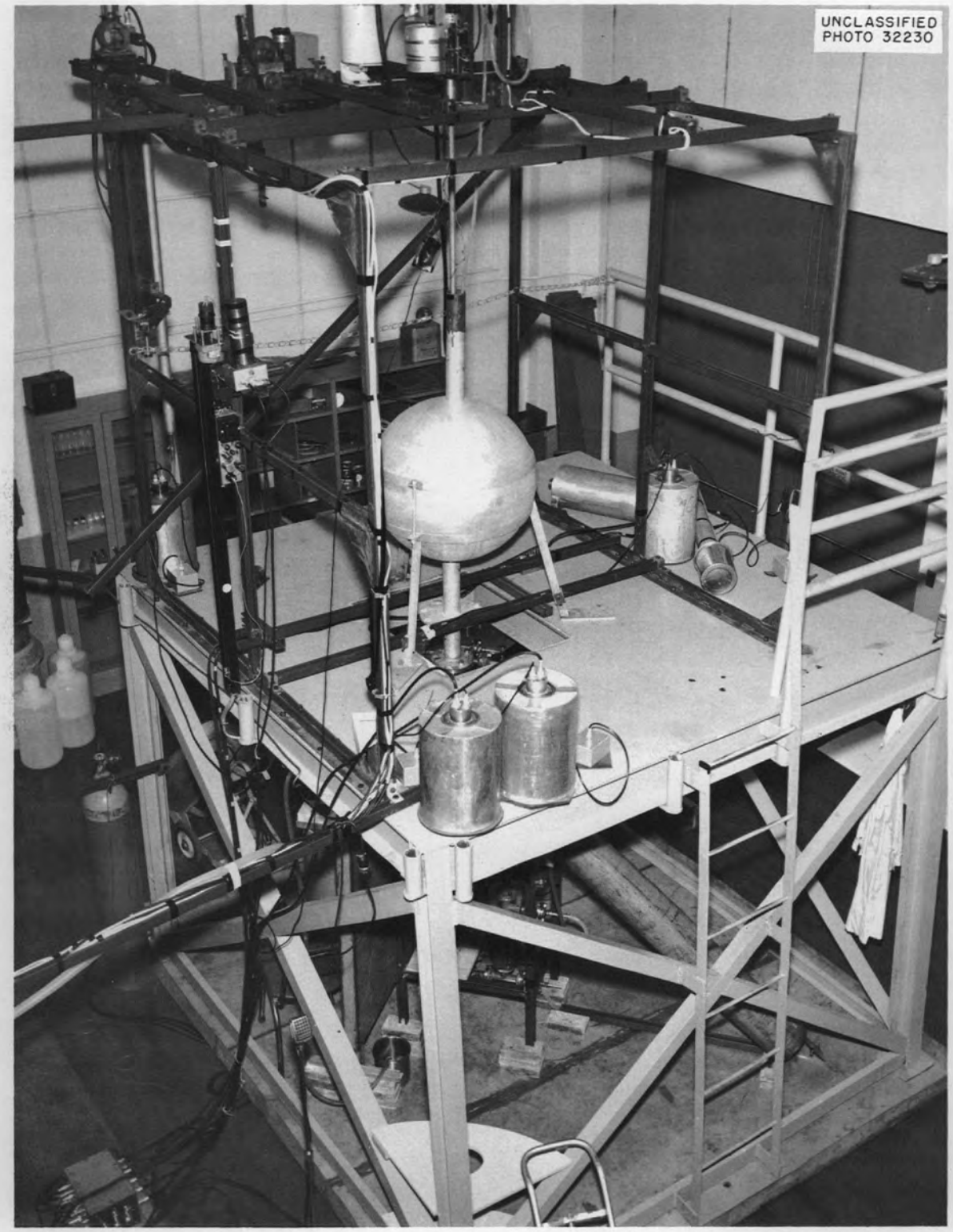

Fig. 12. Experimental Arrangement Utilizing 27-in.-dia Sphere.

A partial spherical shell of aluminum of thickness equal to the nominal thickness of the sphere wall, 0.32 cm, and having an area 32% of that of the sphere was worth 2.3×10^{-4} in reactivity. The reactivity value of solution filling the top polar port was 0.36×10^{-4}. A partial paraffin reflector 8 in. in diameter and 6 in. thick was worth 2.5×10^{-4}. The effective delayed neutron fraction was assumed to be 0.0064 in calculating these reactivities from reactor periods. The critical experiments in this sphere are summarized in Tables 9 and 11 and are listed as Experiments 1 - 9.

48-in.dia Sphere

Hemispherical shells die-formed from type 1100 aluminum plate were welded to form the sphere. Flanged tubes 3 in. in diameter were welded at the poles. Sonic measurements of the wall thickness ranged from 0.26 to 0.35 in. The average thickness, based on the weight of aluminum in the shells, was 0.303 in. (0.77 cm). The capacity, 949.1 liters, was measured by weighing the water contained by the sphere. The volume-averaged diameter was 48.04 in. The outside diameter was measured at 28 places and found to be 48.65 ± 0.09 in. Maximum and minimum values were 48.87 and 48.50 in. The interior surfaces were coated with a phenolic base baked-on enamel to prevent corrosion. The installation is shown in Fig. 13.

Although the reactivity effect of filling the top polar tube with solution was not measured accurately, its value was less than 0.1×10^{-4}. The reactivity effect of the sphere wall was not measured in a manner similar to that with the 27 in. sphere. Since the leakage from this large sphere was about one-third that from the 27-in. sphere, this reactivity effect was expected to be reduced. A 20-in.-dia, 8-in.-thick cylinder of paraffin was used as a reflector control rod and was worth 1.7×10^{-4}. If this value is compared to the result (2.5×10^{-4}) of a similar reflector for the 27 in. sphere, one can conclude that the effect of the container is reduced in the case of this 48-in. sphere.

The critical experiments are summarized in Tables 9 and 11 as Experiments 10 and 11.

5-ft-dia Cylinder

The 5-ft-dia cylinder was fabricated from type 316 stainless steel using machined hoops of mild steel to maintain cylindrical geometry. The internal diameter was measured at 28 places and the average diameter was 60.92 ± 0.05 in. with maximum and minimum values of 61.01 and 60.82 in. The fact that the bottom of the cylinder was slightly dished required an additive correction of 0.25 in. to the observed manometer readings to give the solution height. This correction was evaluated by depth measurements of the liquid in the nominally empty cylinder. A stainless steel reservoir, 1-1/3 x 16 x 8 ft high, provided a safe storage configuration of the solutions used in the 5-ft cylinder. This assembly is shown in Fig. 14.

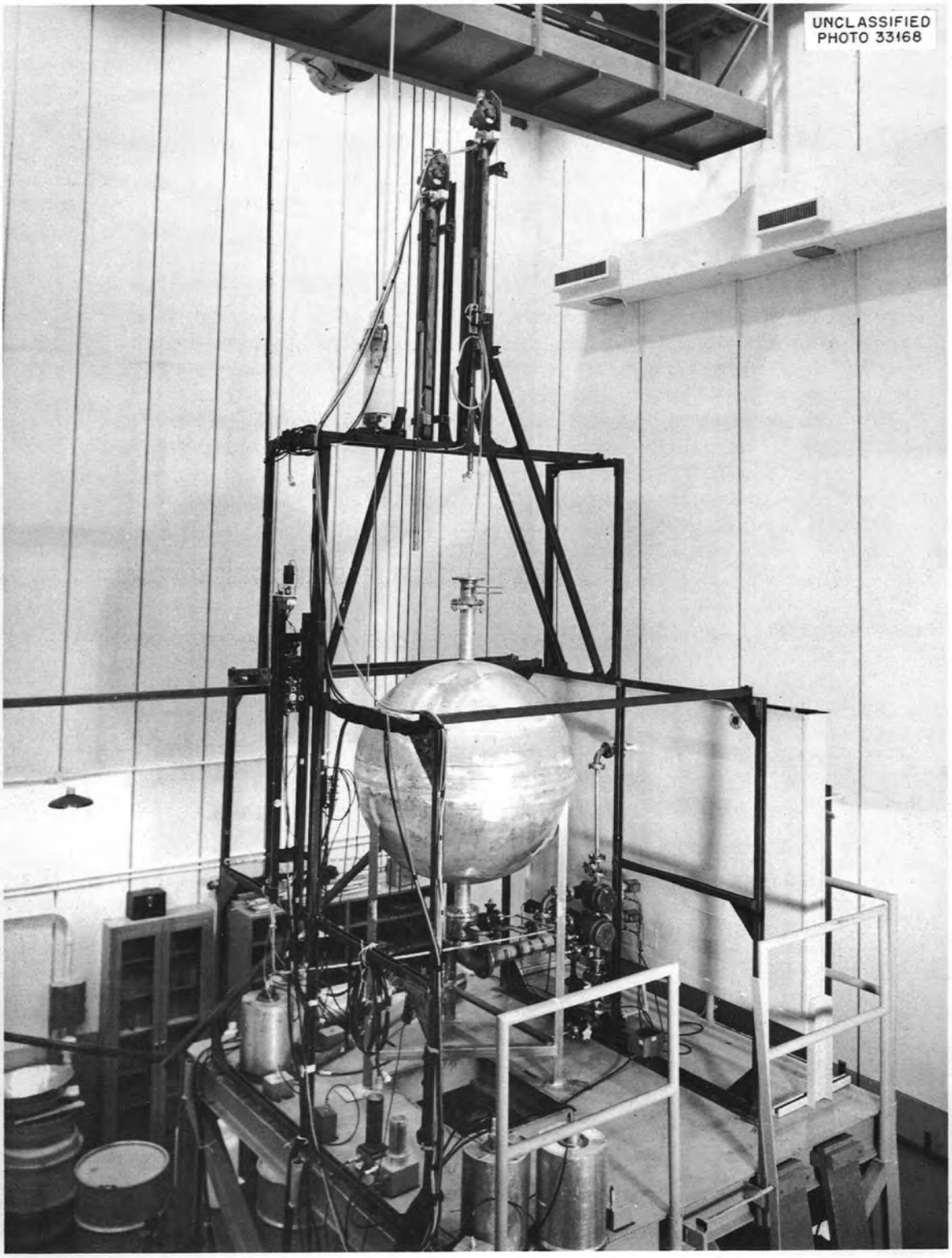

Fig. 13. Experimental Arrangement Employing 48-in.-dia Sphere.

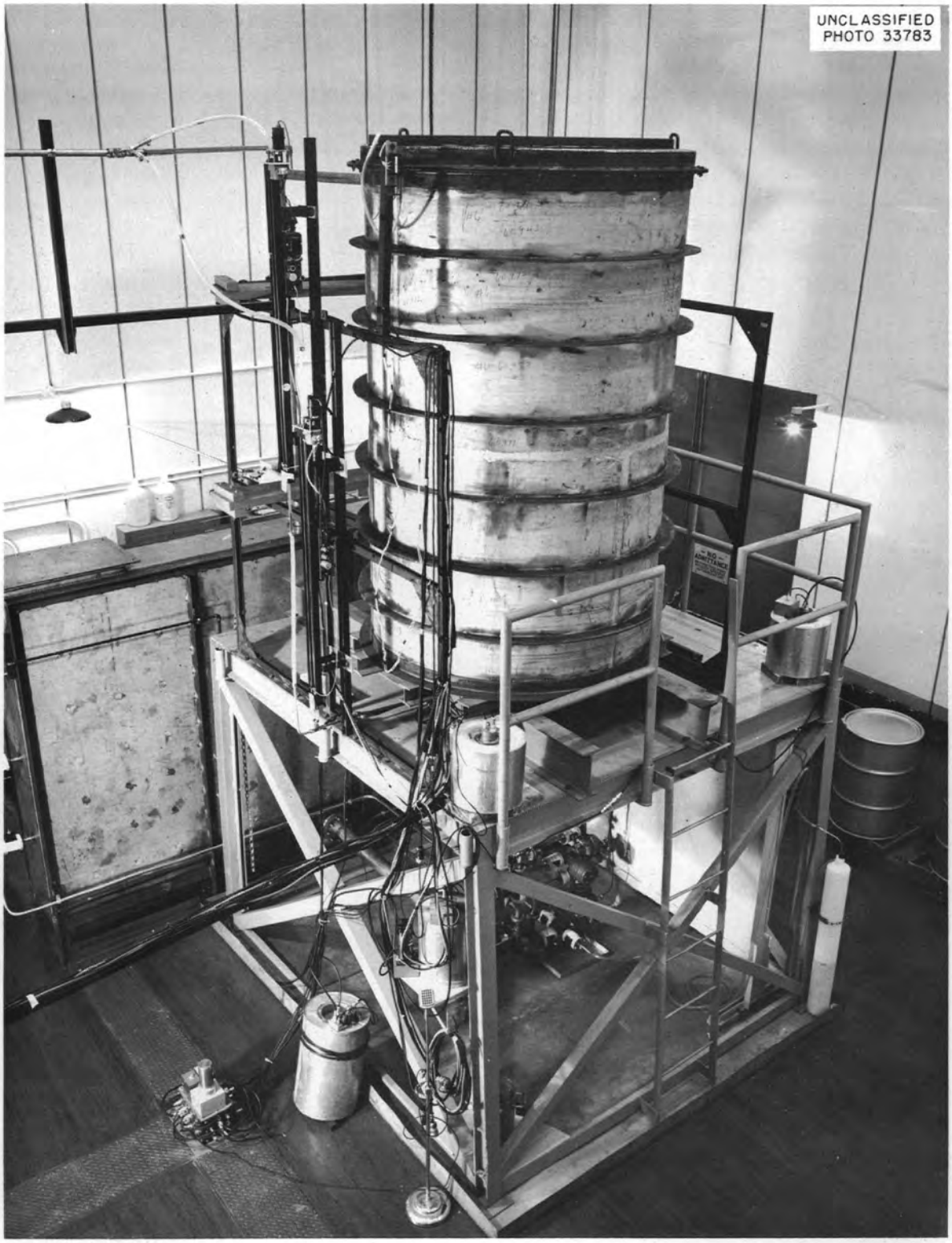

Fig. 14. Experimental Arrangement Utilizing 5-ft-dia Cylinder.

The effect of the tank bottom plate and support beams as a neutron reflector in reducing the critical height was measured by suspending a mock-up of the bottom structures over the top of the solution. By means of a remotely operated crane the mock-up could be lowered to contact with the solution. An electrical probe monitored contact with the solution. The reflector savings obtained at a critical height of 17.25 in. was 0.43 in.; at a critical height of 28.19 in. it was 0.51 in. With the reactor height constant at 27.88 in., the reactivity change accompanying the removal of the mock-up was calculated from stable positive and negative periods. Using the $\partial k/\partial h$ measurements, the height equivalent of this reactivity change was 0.53 in., in close agreement with the critical height change. The latter value of 0.53 in. was used in all the calculations in spite of the measurement of 0.43 in. at a height of 17.25 in. because of more confidence in the latter value. The variance in the reflector savings reduces the confidence that one has in the estimated extrapolation distances from buckling and height measurements. It does not affect the calculated values of eta from these experiments because the bucklings were determined by counter traverses. The critical experiments in this cylinder are summarized in Tables 10 and 11 as experiments 12 - 20.

9-ft-dia Cylinder

The 9-ft-dia cylinder was used for these experiments because it was the largest tank available at the Critical Experiments Facility. It is shown in Fig. 15. This tank was formerly used to contain water moderated and/or reflected assemblies which could be flooded by pumping water into this tank. The associated plumbing was modified to contain a mixing circuit and a means of changing the uranium concentration. Nine control and safety rods, fabricated from 0.026 in. cadmium sheet and encased in stainless steel, were cruciform in cross section with each of the four arms 9 x 96 in. The top of the cylinder was covered by plywood and sheet plastic, with holes for the rod penetrations, to reduce evaporation. This water loss changed the concentration enough to be measurable. During extended experiments water was added in small amounts to maintain the original concentration and hence the critical height. The critical experiments in this cylinder are summarized in Tables 10 and 11 as experiments 21 - 23.

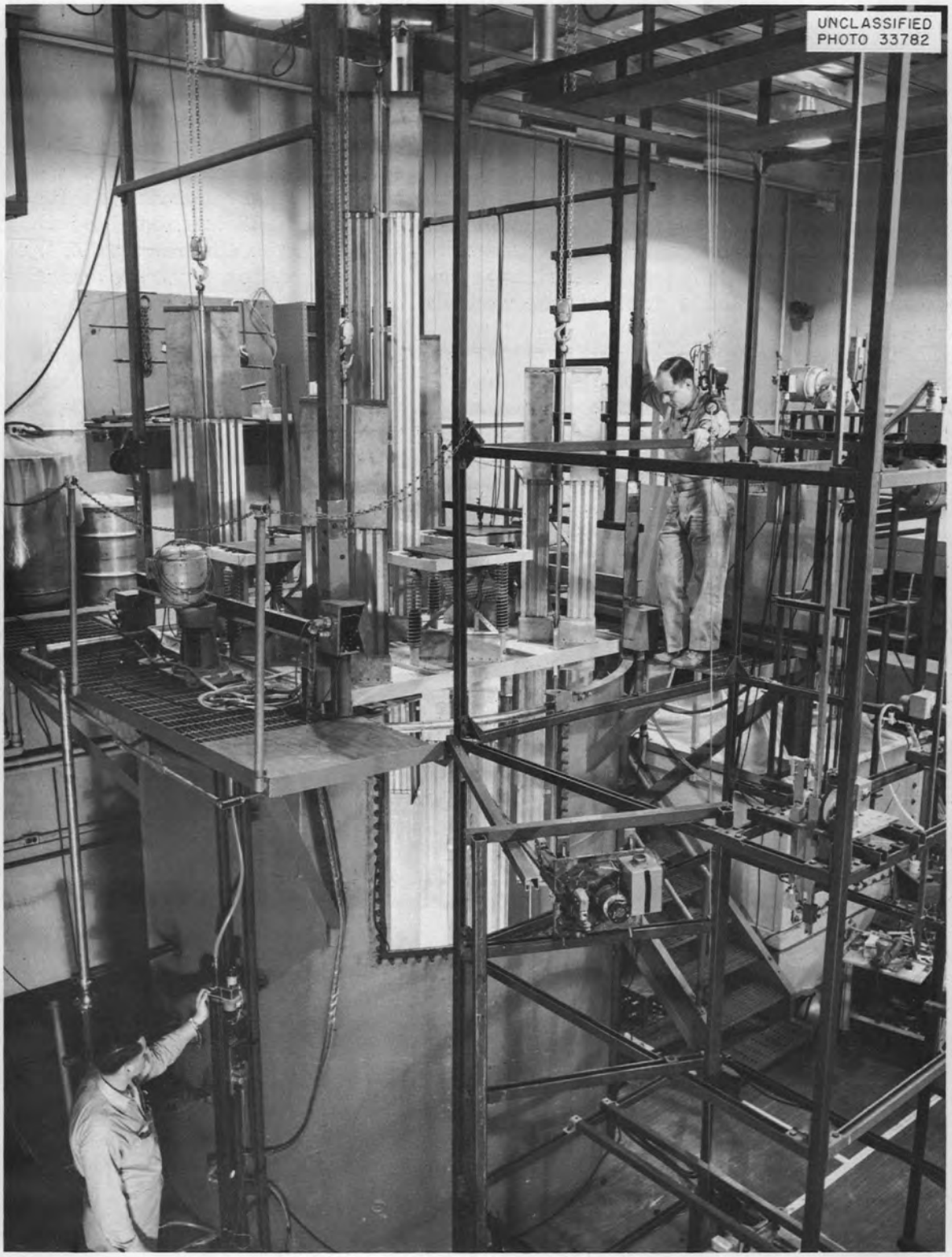

Fig. 15. Experimental Arrangement Using 9-ft-dia Cylinder.

Appendix B

FOIL MEASUREMENTS

U^{233} and U^{235} Foils

The same pair of U^{235} metal foils (93.2% U^{235}), nominally 0.002-in.-thick and 0.3125 in. in diameter, the one bare and the other with a 0.026-in.-thick cadmium cover, were used for all epithermal flux evaluations. This practice eliminated any error which might have existed in the use of several foils of possibly varying characteristics. Each of the foils was sealed in an envelope of Teflon tape with a silicon-base adhesive previously shown to produce no measurable activation. The cadmium cover encased this sandwich. Polyethylene pressure-sensitive tape protected both the cadmium-covered and bare foils during immersion in the uranium solutions.

Oxide foils of U^{233} and U^{235} consisted of a weighed amount of oxide encapsulated in a 0.025-in.-thick, 0.3125-in. ID, 0.500-in.-OD aluminum annulus, with 0.005-in.-thick aluminum top and bottom plates cemented on with epoxy resin. The U^{233}-oxide used in this foils was of high isotopic purity, with gamma-ray background sufficiently low so that it could be used for the activation and be counted by scintillation counters. Oxide foils were protected by polyethylene tape while being exposed.

Activation Techniques

The irradiation time for foil exposures was 20 min., at a power level selected so that foil activities could be compared in two scintillation counters within an hour after irradiation. Pulse height selection was arbitrarily set so that only gamma rays with energies greater than 0.58 Mev were counted. Background counts were made on the foils prior to irradiation to evaluate activity remaining from previous exposures. Foil activity was permitted to decay to relatively low levels before reuse of the foil.

Appendix C

PERIOD OBSERVATIONS

The determination of the nonleakage probability from measurements of the reactor periods induced by height perturbations has been previously detailed. Table 13 contains a complete listing of the many experimental perturbations made in the 5-ft-dia cylinder. Each run number identifies a continuous series of experiments. After the first measurement of each run, height changes in the 12-in.-dia metering reservoir were used to calculate the height change in the 5-ft-dia cylinder, thus improving the precision of measurement of the changes in the solution heights by a factor (24.20) equal to the area ratio between the two vessels. The direct readings of the solution heights are shown in the second column of Table 13. The variation in the metering-tank height indicated in repeated measurements at infinite period reflects a very small drift in the system behavior due probably to inhomogeneities such as bubbles and temperature gradients.

Table 14 presents a similar compendium of height and period data for the 9-ft-dia cylinder. With this system, however, the heights used in the calculations were those observed directly, since no auxiliary vessel was used to improve the precision of the measurements.

Table 13. Period Data for Various Height Perturbations in the 5-ft-dia Cylinder

Run Number	Solution Height (in.) Cylinder	Solution Height (in.) Metering Reservoir	Periods (sec) Ion Chamber No.3	Periods (sec) Ion Chamber No. 4	Periods (sec) Counter No. 1	Periods (sec) Counter No. 2
5A	17.57	32.15	211.9	211.1		
B	17.54	33.08	∞	∞		
C	17.52	33.95	- 297.0	- 290.3		
D	17.57	32.07	184.7	185.8		
E	17.55	33.07	∞	∞		
F	17.52	33.80	- 353.1	- 343.9		
G	17.55	32.63	496.5	487.5		
H	17.54	33.29	- 1043.0	- 995.2		
I	17.55	32.81	967.0	912.7		
J	17.51	34.13	- 248.8	- 240.5		
K	17.57	32.26	246.6	239.0		
M	17.51	34.16	- 256.4	- 240.1		
N	17.58	31.86	156.5	151.4		
O	17.51	34.32	- 180.8	- 207.0		
6H	17.52	34.04	∞	∞		
I	17.54	33.29	300.6			
J	17.53	33.83				
J	17.52	33.97	∞	∞		
J	17.52	33.94				
K	17.50	34.63	- 398.4	- 363.4		
L	17.56	32.98	203.0	198.8		
M	17.52	33.93	∞	∞		
N	17.50	34.72	- 316.7	- 315.1		
21A	28.69	7.78	-	309.4		
B	28.59	10.08	-	∞		
C	-	13.06	-	- 305.1		
D	28.72	6.80	-	202.8		
E	28.47	13.16	-	- 290.7		
F	28.74	6.22	-	167.7		
G	28.59	10.15	-	∞		
22A	28.54	9.36	-	172.1		
B	28.39	13.10	-	∞		
C	28.19	17.99	-	- 186.0		
D	28.62	7.49	-	102.9		
E	28.39	13.11	-	∞		
F	28.16	19.01	-	- 167.3		

Table 13 (Cont.)

Run Number	Solution Height (in.)		Periods (sec)			
			Ion Chamber		Counter	
	Cylinder	Reservoir	No. 3	No. 4	No. 1	No. 2
22G	28.63	7.49	-	100.7		
H	28.39	13.11	-	∞		
I	28.26	16.44	-	-269.0		
J	28.54	9.48	-	174.6		
K	28.39	13.11	-	∞		
L	28.25	16.49	-	261.8		
23A	28.55	14.65	-	124.2		
B	28.36	19.44	-	∞		
C	28.21	22.97	-	-259.3		
D	28.57	14.38	-	117.0		
E	28.36	19.49	-	∞		
F	28.22	22.98	-	-254.7		
G	28.54	14.91	-	133.6		
H	28.36	19.50	-	∞		
I	28.21	22.98	-	-254.2		
46A	41.84	13.98	-	123.1		
B	41.30	27.72	-	∞		
C	40.98	35.68	-	-295.5		
D	41.61	19.87	-	230.3		
E	41.30	-	-	∞		
F	40.93	36.89	-	-265.5		
G	41.60	19.84	-	229.6		
H	41.30	27.88	-	∞		
I	40.93	36.98	-	-263.7		
J	41.61	19.65	-	223.8		
K	41.30	27.84	-	∞		
L	40.93	36.91	-	-263.3		
M	41 71	17.31	-	167.3		
N	41.30	27.80	-	∞		
O	40.93	37.06	-	-264.0		
47A	41.75	10.02	115.2	113.4		
B	41 18	24.59	∞	∞		
C	40.74	35.15	-235.2	-230.3		
D	41.42	18.12	273.2	284.2		
E	41.16	24.69	∞	∞		
G	41.39	18.95	333.2	326.0		
H	41.17	24.66	∞	∞		
I	40.81	33.57	-275.2	-262.9		
J	41.44	17.85	271.6	274.3		

Table 13 (Cont.)

Run Number	Solution Height (in.)		Periods (sec)			
			Ion Chamber		Counter	
	Cylinder	Reservoir	No. 3	No. 4	No. 1	No. 2
47K	41.18	24.64	∞	∞		
L	40.78	34.48	-237.4	-237.4		
M	41.33	20.32	456.3	454.0		
N	41.18	24.53	∞	∞		
O	40.80	34.05	-247.7	-245.5		
51A	41.68	10.02	146.7	142.3		
B	41.20	22.24	-	∞		
C	40.79	32.56	-230.3	-233.2		
D	41.54	13.51	204.3	206.1		
E	41.20	22.32	-	∞		
F	40.80	32.34	-249.9	-242.6		
G	41.60	11.90	168.2	166.6		
H	41.20	22.35	-	∞		
I	40.61	36.84	-190.1	-179.6		
J	41.56	13.13	193.4	190.8		
57B	41.48	20.82	-	∞		
C	40.95	33.97	-179.3	-193.4		
D	41.95	8.99	149.1	149.2		
E	41.48	20.89	∞	∞		
F	41.18	28.35	-316.5	-311.5		
G	41.73	14.38	297.0	295.5		
H	41.48	20.86	∞	∞		
I	41.04	31.87	-230.9	-225.3		
J	41.97	8.60	146.5	144.1		
K	41.49	20.87	∞	∞		
L	40.94	34.13	-198.3	-192.7		
M	41.86	11.38	191.2	190.5		
67A	79.98	-	∞	∞		
B	78.02	-	-302.8	-		
C	83.20	-	157.2	159.5		
D	80.01	-	∞	∞		
E	78.41	-	-370.8	-366.7		
F	82.53	-	198.5	197.7		
G	80.03	-	∞	∞		
H	78.19	-	-322.3	-322.3		
68A	79.94	-	∞	∞		
B	78.50	-	-409.2	-412.9		
C	81.48	-	335.4	331.0		

Table 13 (Cont.)

Run Number	Solution Height (in.) Cylinder	Reservoir	Periods (sec) Ion Chamber No. 3	No. 4	Counter No. 1	No. 2
68D	79.95	-	∞	∞		
E	78.45	-	-391.1	-394.0		
F	82.03	-	247.0	246.1		
G	78.02	-	-304.9	-307.8		
69A	79.78	-	∞	∞		
B	78.48	-	-452.0	-432.4		
C	81.74	-	264.4	259.1		
D	79.78	-	∞	∞		
E	77.71	-	-291.2	-293.4		
F	82.43	-	187.6	184.3		
G	78.00	-	-328.1	-326.5		
H	81.04	-	420.0	415.0		
I	79.78	-	∞	∞		
J	77.51	-	-266.5	-267.3		
			Average of 3 and 4			
80A	18.44	6.86	∞			
B	18.46	6.06	275.6			
C	18.41	7.66	-359.1			
E	18.44	6.89	∞			
F	18.40	7.91	-287.0			
G	18.49	5.39	134.4			
H	18.41	7.69	-365.2			
I	18.44	6.53	620.0			
J	18.42	7.45	-510.0			
K	18.43	6.63	790.6			
L	18.43	6.94	∞			
M	18.41	7.62	-408.4			
81A	18.41	6.63	∞			
B	18.35	8.12	-203.4			
C	18.44	5.42	176.5			
D	18.41	6.65	∞			
E	18.37	7.51	-332.5			
F	18.42	5.83	270.4			
G	18.41	6.67	∞			
H	18.39	7.22	-506.0			
I	18.41	6.23	527.6			
J	18.40	6.68	∞			

Table 13 (Cont.)

Run Number	Solution Height (in.) Cylinder	Reservoir	Periods (sec) Ion Chamber No. 3	No. 4	Counter No. 1	No. 2
			Average of 3 and 4			
81K	18.33	8.54	-174.6			
L	18.46	5.03	123.4			
M	18.34	8.38	-186.1			
N	18.47	4.66	96.2			
O	18.41	6.70	∞			
P	18.36	8.06	-223.7			
97A	19.26	0.84	-		-	-
B	19.25	1.82	∞		∞	∞
C	19.23	2.56	-		-272.8	-267.5
D	19.25	1.16	197.7		198.8	196.0
E	19.25	1.82	∞		∞	∞
F	19.23	2.57	-		-280.8	-269.7
G	19.25	1.16	189.7		191.0	187.6
H	19.25	1.84	∞		∞	∞
I	19.24	2.28	-411.3		-426.6	-419.2
J	19.25	1.47	373.8		382.1	375.5
K	19.25	1.85	∞		∞	∞
L	19.24	2.20	-494.0		-521.4	-511.7
M	19.25	1.38	276.0		297.1	287.3
N	19.25	1.86	∞		∞	∞
O	19.23	2.71	-		-236.6	-235.8
P	19.26	1.01	154.9		151.9	151.2
Q	19.25	1.86	∞		∞	∞
R	19.24	2.24	-319.4		-330.7	-323.2
98A	19.23	2.38	-413.4	-405.3		
B	19.24	1.48	304.2	299.0		
C	19.24	1.94	∞	∞		
D	19.22	2.60	-293.4	-286.3		
E	19.25	1.27	195.6	193.0		
F	19.24	1.94	∞	∞		
G	19.23	2.20	-686.7	-668.2		
H	19.24	1.69	566.4	564.3		
I	19.24	1.95	∞	∞		
J	19.21	3.00	-208.6	-202.8		
K	19.25	0.97	121.0	120.6		
L	19.24	1.96	∞	∞		

Table 13 (Cont.)

Run Number	Solution Height (in.) Cylinder	Solution Height (in.) Reservoir	Periods (sec) Ion Chamber No. 3	Periods (sec) Ion Chamber No. 4	Periods (sec) Counter No. 1	Periods (sec) Counter No. 2
			Average of 3 and 4			
99A	19.25	4.50	∞		∞	∞
B	19.25	4.09	337.9		349.5	343.0
C	19.23	4.98	-360.7		-380.3	-372.8
D	19.24	4.25	567.8		577.1	564.1
E	19.24	4.50	∞		∞	∞
F	19.22	5.35	-232.5		-240.5	-236.2
G	-	3.65	144.1		151.5	149.0
H	19.24	4.91	430.9		442.9	437.3
I	19.25	4.50	∞		∞	∞
J	19.25	4.20	471.1		483.3	471.9
K	19.22	5.53	-196.2		-204.9	-199.2
L	19.26	3.78	176.0		182.4	179.4
M	19.24	4.96	-378.1		-392.9	-386.9
O	19.24	4.50	∞		∞	∞
102A	23.07	4.42	∞	∞	∞	∞
B	23.08	4.05	608.4	619.3	659.9	637.1
C	23.03	5.56	-272.1	-267.7	-269.3	-265.1
D	23.10	3.32	180.4	181.1	184.9	181.9
E	23.06	4.83	-698.6	-684.5	-723.5	-710.3
F	23.06	4.48	∞	∞	∞	∞
G	23.07	4.00	486.0	478.1	495.3	486.0
H	23.04	5.29	-353.1	-354.7	-361.5	-354.8
I	23.10	3.08	134.7	134.4	140.5	138.0
J	23.07	4.51	∞	∞	∞	∞
K	-	5.00	-557.7	-549.8	-575.0	-564.8
103A	23.07	3.02	∞	∞	∞	∞
B	23.00	4.68	-192.7	-	-202.7	-200.9
C	23.10	1.43	117.0	115.9	122.6	119.0
D	23.06	3.05	∞	∞	∞	∞
E	23.03	4.02	-315.1	-302.6	-318.8	-313.0
F	23.08	2.06	206.1	204.6	210.2	205.8
G	-	3.07	∞	∞	∞	∞
H	23.05	3.57	-565.0	-570.4	-583.3	-572.3
I	23.07	2.52	434.6	423.7	441.5	433.2
J	23.06	3.09	∞	∞	∞	∞
K	23.02	4.36	-252.8	-250.6	-254.2	-249.4
L	23.09	1.84	163.0	160.4	166.7	164.5
M	23.06	3.12	∞	∞	∞	∞
N	23.00	4.64	-216.4	-214.3	-216.4	-213.7
O	23.09	1.56	121 3	123.0	125.4	124.0

Table 13 (Cont.)

Run Number	Solution Height (in.) Cylinder	Reservoir	Periods (sec) Ion Chamber No. 3	No. 4	Counter No. 1	No. 2
			Average of 3 and 4		Average of 1 and 2	
104A	23.07	4.50	∞		∞	
B	23.07	4.08	635.6		650.2	
C	23.05	5.10	-442.9		-457.6	
D	23.08	3.69	294.0		290.9	
E	23.07	4.45	∞		∞	
F	23.04	5.36	-334.6		-345.3	
G	23.07	4.50	∞		∞	
H	23.03	5.54	-289.7		-293.8	
I	23.09	3.24	165.8		167.6	
J	23.03	5.55	-284.2		-291.0	
K	23.07	3.84	358.1		361.8	
L	23.06	4.46	∞		∞	
105A	23.08	6.47	∞	∞	∞	∞
B	23.02	7.93	-217.3	-217.3	-224.3	-217.9
C	23.10	5.04	135.8	133.6	138.9	135.7
D	23.08	6.46	∞	∞	∞	∞
E	23.04	7.46	-304.2	-303.8	-318.0	-308.7
F	23.09	5.49	217.3	213.7	220.0	216.1
G	23.08	6.47	∞	∞	∞	∞
H	23.05	7.18	-412.9	-398.7	-416.4	-408.6
I	23.08	5.80	330.3	327.7	337.6	331.7
J	23.07	6.47	∞	∞	∞	∞
K	22.99	8.41	-179.5	-181.4	-182.6	-178.3
L	23.12	4.58	94.2	93.4	95.1	94.2
			Average of 3 and 4		Average of 1 and 2	
111A	30.36	7.28	∞		∞	
B	30.32	8.34	-528.7		-535.6	
C	30.36	6.34	449.2		460.1	
D	30.36	7.39	∞		∞	
E	30.30	8.92	-375.7		-384.1	
F	30.38	5.87	285.7		287.7	
G	30.36	7.44	∞		∞	
H	30.26	10.06	-241.2		-243.6	
I	30.42	4.97	164.3		166.7	
J	30.35	7.50	∞		∞	
K	30.23	10.78	-206.4		-204.4	
L	30.45	4.24	116.6		118.1	

Table 13 (Cont.)

Run Number	Solution Height (in.) Cylinder	Solution Height (in.) Reservoir	Periods (sec) Ion Chamber No. 3	Periods (sec) Ion Chamber No. 4	Periods (sec) Counter No. 1	Periods (sec) Counter No. 2
			Average of 3 and 4		Average of 1 and 2	
111M	30.36	7.52	∞		∞	
N	30.28	9.51	-309.7		-310.5	
O	30.41	5.29	184.7		185.9	
P	30.35	7.57	∞		∞	
112A	30.41	5.30	-		-	
B	30.34	7.71	∞		∞	
C	30.37	6.04	267.7		-	
D	30.28	9.07	-415.5		-432.0	
E	30.31	7.78	∞		∞	
F	30.39	5.76	219.9		226.5	
G	30.24	10.08	-266.2		-271.7	
H	30.42	4.84	134.5		137.0	
I	30.26	9.22	-396.6		-401.5	
J	30.30	7.94	∞		∞	
K	30.39	5.52	185.1		187.9	
L	30.27	9.48	-357.0		-364.3	
M	30.41	5.09	144.5		147.6	
N	30.33	7.86	∞		∞	
O	30.24	10.36	-251.0		-257.5	
P	30.40	5.34	159.7		163.6	
Q	30.33	7.88	∞		∞	
R	30.26	9.76	-321.6		-325.9	
113A	30.34	7.49	∞		∞	
B	30.35	6.34	401.2		408.4	
C	30.34	7.48	∞		∞	
D	30.29	8.83	-429.5		-442.3	
E	30.37	6.21	358.0		365.7	
F	30.33	7.48	∞		∞	
G	30.26	9.53	-297.0		-307.4	
I	30.33	7.48	∞		∞	
J	30.26	9.53	-298.5		-306.1	
K	-	5.32	-194.3		-196.9	

Table 13 (Cont.)

Run Number	Solution Height (in.) Cylinder	Reservoir	Periods (sec) Ion Chamber No. 3	No. 4	Counter No. 1	No. 2
			Average of 3 and 4		Average of 1 and 2	
122X	16.17	3.37	-		-	
A	54.40	16.94	∞		-	
B	54.55	12.86	593.0		-	
C	54.09	24.91	-362.1		-	
D	54.70	9.04	281.2		-	
E	54.25	20.89	-680.1			
F	54.38	16.90	∞		-	
G	54.53	13.31	659.0		-	
H	53.99	27.29	-289.4		-	
I	54.82	6.29	198.6		-	
J	54.16	23.34	-427.4		-	
K	54.38	16.85	∞		-	
123A	54.44	17.24	∞		-	
B	54.58	12.76	543.3		-	
C	54.26	21.89	-590.0		-	
D	54.70	9.93	306.2		-	
E	54.14	24.53	-393.9		-	
F	54.44	17.31	∞		-	
G	54.54	13.82	706.8		-	
H	54.31	20.78	-749.1		-	
I	54.67	10.76	347.0		-	
J	54.44	17.19	∞		-	

Table 14. Period Measurements in 9-ft-dia Cylinder

Date	Solution Height (in.) Probe	Liquid Level	Periods (sec) Count Rate Meter	Logarithmic Amplifier	Counter 1	Counter 2
4-30-59	47.78[a]	47.76	209	194		
	47.24	47.24	∞	∞		
	48.21	48.22	96	97.8		
	47.235	47.22	∞	∞		
	46.20	46.19	- 146	- 148		
	47.775	47.78	192	184.6		
	47.205	47.24	∞	∞		
	46.72	46.76	- 295	- 285		
	47.52	47.53	382	351		
	47.205	47.20	∞	∞		
	46.415	-	185	- 187		
	48.20	-	98	92.4		
	47.205	47.22	∞	∞		
	46.18	46.21	- 147.7	- 155.8		
5-4-59	46.88[a]	-	195.5	192.5	192.4	
	46.36	-	∞	∞	∞	
	45.84	-	254	- 248	- 254.5	
	46.87	-	181	187	186	
	46.32	-	∞	∞	∞	
	45.82	-	- 207	- 266	- 262.5	
	46.60	-	401	375	373	
	46.31	-	∞	∞	∞	
	46.06	-	- 476	- 483	- 492	
	47.0	-	142	135	134.45	
	46.30	-	∞	-	∞	
	45.59	-	- 191	- 190.5	- 195.15	
	47.21	-	-	98.0	99.93	
	46.29	-	∞	∞	∞	
	45.32	-	151.5	- 148	- 151.2	
5-7-59	99.67[a]	-	137.5	139.7	143.75	
	94.26	-	∞	∞	∞	
	90.28	-	- 234	- 235.5	- 237	
	97.73	-	227.5	212	218.5	
	94.14	-	∞	∞	∞	
	90.57	-	- 259	- 254	- 264	
	96.15	-	371	370.5	367	
	93.92	-	∞	∞	∞	
	91.21	-	- 327	- 352	- 312	
	99.83	-	119.5	119.5	122.8	
	93.78	-	∞	∞	∞	
	89.80	-	- 291	- 236	- 237.6	

Table 14. Contd.

Date	Solution Height (in.) Probe	Liquid Level	Periods (sec) Count Rate Meter	Logarithmic Amplifier	Counter 1	Counter 2
5-15-59	99.76[a]	-	Out	178	178.9	178.5
	95.23	-	-	∞	∞	∞
	90.27	-	-	- 192	- 202.5	- 195.2
	98.24	-	-	268	268.9	268.4
	95.155	-	-	∞	∞	∞
	92.08	-	-	- 308	- 313.4	- 314.5
	97.66	-	-	315	312.5	314.0
	95.01	-	-	∞	∞	∞
	92.52	-	-	- 377	- 382.9	- 381.7
	98.57	-	-	217.3	218.2	214.9
	94.79	-	-	∞	∞	∞
	91.17	-	-	- 263.5	- 265.1	- 264
	97.83	-	-	263.5	266.4	262.9
	94.75	-	-	∞	∞	∞
	92.755	-	-	- 465	- 471.9	- 467.5
	94.65[a]	-	234	225	-	231
	91.45	-	∞	∞	∞	∞
	88.48	-	- 306.5	- 295.5	- 303	- 294.7
	93.33	-	396	391	394	391.1
	91.37	-	∞	∞	∞	∞
	89.37	-	- 438	- 426	- 424.7	- 427.2
	96.10	-	153	144.2	154.8	148.2
	91.32	-	∞	∞	∞	∞
	87.79	-	- 256	- 254	- 256.7	- 249.6
	95.08	-	187	181	198.8	191.1
	91.28	-	∞	∞	∞	∞
	88.63	-	- 324	- 324	- 348.9	- 326.2
	93.68	-	-	304	-	306.5
	91.23	-	∞	∞	∞	∞
	86.44	-	-	-	-	- 193.4

Date	Probe	Logarithmic Amplifier	Logarithmic Amplifier	Counter 1	Counter 2
5-20-59	99.94[a]	143.8	143	142.4	143.9
	94.54	∞	∞	∞	∞
	98.90	- 215	- 211.5	- 215.1	- 216.6
	98.96	178	175.5	177.8	178.9
	94.50	∞	∞	∞	∞
	91.48	- 309.5	- 303	- 316.6	- 318.4
	98.0	230	232.5	230.2	230.6
	94.44	∞	∞	∞	∞

Table 14. Cont'd

Date	Probe	Logarithmic Amplifier	Logarithmic Amplifier	Counter 1	Counter 2
5-20-59	90.54	- 248.8	245.5	- 248.3	- 249.5
	96.92	345	343	340.3	343.9
	94.44	∞	∞	∞	∞
	91.99	- 373	- 365	- 372.3	- 374.3
7-27-59	35.44[b]	∞		∞	∞
	35.66	214		221	223
	35.43	∞		∞	∞
	35.22	- 289		- 287	- 294
	35.815	118		125	123
	34.94	- 145		- 157	- 149
	35.44	∞		∞	∞
	35.08	- 189		- 182	- 186
	35.56	429		468	466
7-28-59	35.785	120.4		121	121
	35.41	∞		∞	∞
	34.985	- 166		- 167	- 168
	35.53	168		446	450
	35.41	∞		∞	∞
	35.205	- 277		- 308	- 312
	35.625	232		230	233
	35.41	∞		∞	∞
	35.08	- 196		-	-
	35.63	228		237	239
	35.41	∞		∞	∞
	35.06	- 207			
7-30-59	34.995	- 201.5	- 208.1	- 206.9	- 207.8
	35.665	140.4	137.4	143.4	144.2
	35.065	- 248.1	- 267.6	- 252.4	253.9
	35.565	204.3	202.1	207.9	208.7
	34.925	- 173.3	- 174.9	- 174.6	- 177.0
	35.725	115.9	135.8	116.3	115.7
	35.10	- 276.0	- 278.9	- 271.3	- 274.0
	35.560	220.56	218.4	221.4	222.2
	34.825	147.0	150.7	- 144.2	- 144.1

a. Solution height = probe height + 0.67 in.
b. Solution height = probe height + 0.43 in.

REFERENCES

1. J. T. Thomas, J. K. Fox, and A. D. Callihan, A Direct Comparison of Some Nuclear Properties of U^{233} and U^{235}, Nucl. Sci. Engr. 1, 20 (1956).

2. W. E. Kinney, et al., Appl. Nuclear Phys. Ann. Rep. Sept. 10, 1956, ORNL-2081, p. 133.

3. A. M. Weinberg and E. P. Wigner, The Physical Theory of Neutron Chain Reactors, University of Chicago Press, Chicago, 1958, p. 381 ff.

4. R. Gwin, A. M. Weinberg and D. K. Trubey, Proc. U. N. Intern. Conf. Peaceful Uses of Atomic Energy, 2nd, Geneva, 1958 12, 529 (1958).

5. M. J. Poole, A Measurement of the Neutron Spectra in Moderators and Reactor Lattices, J. Nuclear Energy 5, 325 (1957).

6. R. S. Stone and R. E. Slovacek, Neutron Spectra Measurements, KAPL-1916 (Sept. 15, 1957).

7. J. Certaine and R. Aronson, Distribution of Fission Neutrons in H_2O at Indium Resonance Energy, NDA-15-C-40 (June 15, 1954).

8. D. W. Magnuson, R. Gwin and W. E. Kinney, Neutron Phys. Ann. Prog. Rep. Sept. 1, 1959, ORNL-2842, p. 151.

9. D. W. Magnuson and R. Gwin, Trans. Am. Nuclear Soc., 2 (1) 146 (1959).

10. G. J. Safford and W. W. Havens, Jr., A Critical Review of the Cross Section and Fission Parameters of U^{235} Below 1 ev, WASH-1022 (May 18, 1959).

11. J. A. Harvey, personal communication, Oct. 23, 1959.

12. C. H. Wescott and D. A. Roy, Supplement to Effective Cross Section Values for Well-Moderated Thermal Reactor Spectra, CRRP-862 (AECL-869) (Aug. 20, 1959).

13. D. J. Hughes, R. B. Schwartz, Neutron Cross Sections 2nd Ed., BNL-325 (July 1, 1958), and
D. J. Hughes, B. A. Magurno, and M. K. Brussel, Neutron Cross Sections, 2nd Ed. Supplement 1, (Jan. 1, 1960).

14. W. E. Kinney, private communication of ORACLE calculations.

15. J. A. Harvey, Phys. Ann. Prog. Rep. Mar. 10, 1959, ORNL-2718.

16. D. K. Trubey, private communication, July 30, 1959.

17. Reactor Physics Constants, ANL-5800 (1958).

18. D. K. Trubey, H. S. Moran, A. M. Weinberg, Appl. Nuclear Phys. Ann. Prog. Rep. Sept. 1, 1957, ORNL-2389, p. 159.

19. R. R. Coveyou and J. G. Sullivan, Neutron Phys. Div. Ann. Prog. Rep. Sept. 1, 1958, ORNL-2609, p. 82.

20. Keepin, Wimett and Zeigler, Phys. Rev. 107, 1044 (1957).

21. Recent values by Kenward and Sanders, and Diven, et al., quoted by Safford and Havens, WASH-1022 (May 18, 1959).

22. R. R. Coveyou amd J. G. Sullivan, unpublished calculations, 1959.

23. R. Gwin and D. W. Magnuson, Determination of η by Comparison of $\eta\sigma_a$ of U^{233} and Pu^{239} with $\eta\sigma_a$ of U^{235} in a Flux Trap Critical Assembly, ORNL-CF-60-4-11 (1960).

24. R. L. Macklin, G. deSaussure, et al., Manganese Bath Measurements of η of U^{233} and U^{235}, ORNL CF-60-2-84 (1960).

25. E. V. Haake, A Sensitive BF_3 Ionization Chamber, NEPA-1742 (April 4, 1951).

INTERNAL DISTRIBUTION

1. F. S. Alsmiller
2. E. P. Blizard
3. T. V. Blosser
4. V. R. Cain
5-14. A. D. Callihan
15. G. T. Chapman
16. G. deSaussure
17. L. Dresner
18. W. K. Ergen
19. G. M. Estabrook
20. J. K. Fox
21. L. W. Gilley
22-71. R. Gwin
72. J. A. Harvey
73. K. M. Henry
74. L. B. Holland
75. J. L. Hull
76. E. B. Johnson
77. W. H. Jordan
78. P. Kasten
79. J. D. Kington
80. J. Lewin
81. T. A. Love
82. R. L. Macklin
83. R. E. Maerker
84-133. D. W. Magnuson
134. F. C. Maienschein
135. J. T. Mihalczo
136. F. J. Muckenthaler
137. R. W. Peelle
138. A. M. Perry
139. E. G. Silver
140. A. Simon
141. J. T. Thomas
142. D. K. Trubey
143. V. V. Verbinski
144. D. R. Ward
145. A. M. Weinberg
146. W. Zobel
147. R. Perez-Belles
148. M. J. Skinner
149. E. Inonu
150. Central Research Library
151-160. Laboratory Records Department
161. Laboratory Records, ORNL, R.C.
162. Technical Information Service, AEC

EXTERNAL DISTRIBUTION

163. C. L. Schuske, Dow Chemical Company, Denver, Colorado
164. H. K. Clark, E. I. DuPont de Nemours and Company, Aiken, South Carolina
165. F. E. Woltz, Goodyear Atomic Corporation, Portsmouth, Ohio
166-167. J. E. Faulkner and E. D. Clayton, Hanford Atomic Products Operation, Richland, Washington
168-171. H. C. Paxton, G. R. Keepin, G. Hansen and B. Diven, Los Alamos Scientific Laboratory, Los Alamos, New Mexico
172. H. Zeitz, National Lead of Ohio, Cincinnati, Ohio
173-177. W. B. Lewis, D. R. DeBoisblanc, J. E. Evans, R. G. Fluharty and D. G. Reid, Phillips Petroleum Company, Idaho Falls, Idaho
178-179. J. E. Carothers and F. Kloverstrom, University of California Radiation Laboratory, Livermore, California
180. R. V. Meghreblian, Jet Propulsion Laboratory, Pasadena, California
181. C. E. Center, Union Carbide Nuclear Company, ORGDP
182. H. F. Henry, Union Carbide Nuclear Company, ORGDP
183. J. D. McLendon, Union Carbide Nuclear Company, Y-12

184. O. W. Hermann, Union Carbide Nuclear Company, Paducah Plant
185. J. L. Fowler, Chairman, Nuclear Cross Sections Advisory Group, Oak Ridge National Laboratory, Oak Ridge, Tennessee
186. R. A. Charpie, Chairman, Advisory Committee on Reactor Physics, ORNL, Oak Ridge, Tennessee
187. A. F. Henry, Westinghouse Electric Company, Bettis Atomic Power Division, Pittsburgh 30, Pennsylvania
188-189. M. C. Edlund and D. V. P. Williams, Babcock and Wilcox Company, Lynchburg, Virginia
190. J. Chernick, Brookhaven National Laboratory, Upton, L. I., New York
191. E. P. Wigner, Princeton University, Princeton, New Jersey
192. C. O. Muehlhause, National Bureau of Standards, Washington 25, D. C.
193. W. H. Zinn, Combustion Engineering, Windsor Locks, Connecticut
194-196. B. I. Spinrad, Walter Kato and D. Okrent, Argonne National Laboratory Lemont, Illinois
197. P. F. Zweifel, Department of Nuclear Engineering, University of Michigan, Ann Arbor, Michigan
198. R. R. Wilson, Cornell University, Ithaca, New York
199. W. W. Havens, Columbia University, New York, N. Y.
200. Herbert Goldstein, Nuclear Development Corporation of America, White Plains, New York
201. Rudolph Sher, Brookhaven National Laboratory, Upton, L. I., New York
202. B. J. Toppel, Argonne National Laboratory, Lemont, Illinois
203. W. B. Henderson, General Electric Company, Cincinnati, Ohio